Thesis

Epigenetic modification of cardiac function

Submitted by

Katharina Scharer

to obtain the academic degree of

Doctor of medicine

(Dr. med. univ.)

at the

Medical University of Graz

performed at the

Division of Cardiology

Department of Internal Medicine

under the guidance of

Research Prof. Priv.-Doz. Dr.med. Dr.scient.med. Markus Wallner

and

Dr.med.univ. Dr.scient.med. Ewald Kolesnik

Graz, 05.06.2023

Statutory Declaration

I declare on my honour that I have written this thesis independently and without assistance, I have not used other than the specified sources and parts taken from other sources, verbatim or in substance have been identified as such.

Graz, 05.06.2023 *Katharina Scharer eh.*

Acknowledgments

The development of this thesis took patience, energy, and time. Moreover, the realization of the work relied on help from different people. Consequently, I would like to thank everyone who supported me in any way. A special thanks is given to my supervisor Research Prof. Priv.-Doz. Dr.med. Dr.scient.med. Markus Wallner and Co-supervisor Dr.med.univ. Dr.scient.med. Ewald Kolesnik. They stood behind me with professional advice anytime. As a consequence, I was able to learn the basics of scientific work. Despite some setbacks, they motivated me again and again. Without their advice, I could not have accomplished this thesis so well.

I am also grateful for the smooth cooperation with the division of cardiac surgery. In particular, I would like to accentuate the fruitful cooperation with Ao.Univ.-Prof. Dr.med.univ. Heinrich Mächler, MA MSc. He coordinated the delivery of the human atrial tissue samples for the realization of this unique heart failure model.

I would like to give my greatest thanks to my family and friends, who always supported me during this challenging time. I am incredibly grateful to my parents and grandparents for assisting me during the duration of my study.

Table of Contents

Abbreviations and Definitions

ACC	American College of Cardiology
ACE	Angiotensin-converting enzyme
ADP	Adenosine diphosphate
AHA	American Heart Association
Akt	Protein kinase B
ANOVA	Analysis of variance
ARB	Angiotensin II receptor blockers
ARNI	Angiotensin receptor/neprilysin inhibitor
ATP	Adenosine triphosphate
ATP2A3	ATPase sarcoplasmic/endoplasmic reticulum Ca2+ transporting 3
BDM	2,3-butanedione monoxime
BL	Baseline
BMI	Body Mass Index
Ca^{2+}	Calcium ion
CABG	Coronary Artery Bypass Graft
$CaCl_2$ $2H_2O$	Calcium chloride
CICR	Calcium induced calcium release
cm	Centimetre
CoA	Coenzyme A
COOH	Carboxylic acid
DNA	Deoxyribonucleic acid
Dp/dt_{max}	Kinetic of cardiac muscle contraction
Dp/dt_{min},	Kinetic of cardiac muscle relaxation
DSMO	Dimethylsulfoxide
DSS	Dahl salt-sensitive
ECC	Excitation-contraction coupling
É/e	Indicator of left ventricular diastolic function
EF	Ejection fraction
ELC	Myosin essential light chains
ESC	European Society of Cardiology
$FADH_2$	Reduced form of flavin adenine dinucleotide

FDA	U.S. Food and Drug Administration
Gsk3β	Glycogen synthase kinase-3
HATs	Histone acetyltransferases
HCN	Hyperpolarization-activated cyclic nucleotide-gated
HDAC	Histone deacetylase
HDACi	Histone deacetylase inhibitors
HF	Heart failure
HFA-PEFF	Diagnostic score of heart failure with preserved ejection fraction
HFimpEF	HF with improved ejection fraction
HFmrEF	Heart failure with mid-range EF
HFpEF	Heart failure with preserved ejection fraction
H_2FPEF	Score for Heart Failure with Preserved Ejection Fraction
HFrEF	Heart failure with reduced ejection fraction
HFSA	Heart Failure Society of America
H_2O	Water
Hz	Hertz
I_{Ca}	Voltage-gated calcium channels
I_{Na}	Voltage-gated sodium channels
K^+	Potassium ion
KCl	Potassium chloride
KH_2PO_4	Potassium dihydrogen phosphate
L	Litre
L_{max}	Ideal length between sarcomeres
LA	Left atrium
LV	Left ventricle
LVEDP	Left ventricular enddiastolic pressure
LVEF	Left Ventricular Ejection Fraction
LVH	Left ventricular hypertrophy
mCU	Mitochondrial calcium-uniporter
MgSO4 . 7H2O	Magnesium sulphate heptahydrate
mRNA	Messenger ribonucleic acid
mV	Millivolts
Na^+	Sodium ion

NaCl	Sodium chloride
NAD^+	Nicotinamide adenine dinucleotide
NADH	Nicotinamide adenine dinucleotide + hydrogen
$NaHCO_3$	Sodium bicarbonate
NCE	Mitochondrial sodium/calcium-exchanger
NCX	Sodium-calcium exchanger
NH_2	Amino radical
NHE	Mitochondrial sodium/hydrogen-exchanger
NKA	Sodium-potassium pump
N^+/K^+-ATPase	Sodium-potassium pump
nM	Nanomolar
NT-proBNP	N-terminal pro brain natriuretic peptide
O_2	Oxygen
P_i	Phosphate
pH	Potential of hydrogen
PDH	Pyruvat dehydrogenase
PARADIGM-HF	Prospective Comparison of ARNI with ACEI to Determine Impact on Global Mortality and Morbidity in Heart Failure
PARAGON-HF	Prospective Comparison of ARNI With ARB Global Outcomes in Heart Failure with Preserved Ejection Fraction
PI3K	Phosphoinositide 3-kinases
RC	Respiratory chain
RLC	Myosin regulatory light chains
RT 50%	Relaxation parameter
RyR	Ryanodine receptor
RyR1	Ryanodine receptor type 1
RyR2	Ryanodine receptor type 2
SA	Sinoatrial
SAHA	Suberoylanilide hydroxamic acid
SEM	Standard error of the mean
SERCA	Sarcoplasmic reticulum calcium-ATPase
SERCA2	Sarcoplasmic reticulum calcium-ATPase enzyme 2

SERCA3	Sarcoplasmic reticulum calcium-ATPase enzyme 3
$SGLT_2$	Sodium-glucose cotransporter-2
$SGLT_2i$	Sodium-glucose cotransporter-2 inhibitor
SIRT	Sirtuins
SR	Sarcoplasmic reticulum
TCA	Tricarboxylic acid
VOCCs	Voltage-operated Ca2+ channels
β-MyHC	Myosin heavy chain beta
Δψm	Electrical gradient
μM	Micromolar

List of Figures

List of Table

Zusammenfassung

Hintergrund:

Die Herzinsuffizienz (HF) stellt ein weltweites Gesundheitsproblem dar mit hoher Prävalenz und ist verbunden mit hoher Morbidität und Mortalität. In Europa sind allein knapp 14 Millionen PatientInnen betroffen. In Österreich leiden ungefähr 1-2% der Gesamtbevölkerung an einer chronischen Herzinsuffizienz, wobei fast 14.000 Menschen jährlich an dieser Erkrankung sterben. Ungefähr die Hälfte aller Herzinsuffizienz PatientInnen leiden an Herzinsuffizienz mit erhaltener Ejektionsfraktion (HFpEF). Die charakteristischen Eigenschaften der HFpEF sind linksventrikuläre Hypertrophie (LVH), erhöhter linksventrikulärer enddiastolischer Druck (LVEDP), Vergrößerung des linken Atriums, sowie erhöhte NT-proBNP Werte, während die Ejektionsfraktion erhalten bleibt. Diese Veränderungen gehen mit folgenden klinischen Symptomen einher Leistungsminderung, Müdigkeit, Abgeschlagenheit, Dyspnoe und Ödeme. Während es für Herzinsuffizienz mit reduzierter Ejektionsfraktion (HFrEF) eine mehrere Therapiemöglichkeiten gibt, basiert die Behandlung von HFpEF weitgehend auf symptomatischer Therapie. Bisher konnte nur unter Natriumglukose Kotransporter 2 (SGLT2) -Inhibitoren die Prognose von HFpEF PatientInnen verbessert werden. Deshalb werden Alternativen dringend benötigt.

HDACs sind Enzyme, die durch posttranslationale Modifikation der Histon-Proteine eine entscheidende Rolle in der Regulation der Genexpression spielen. HDAC-Inhibitoren (HDACi) werden bisher in der Behandlung von T-Zell Lymphomen eingesetzt. In diversen präklinischen Studien zeigten HDACi positive Effekte auf die myofibriläre Relaxation. Die zu Grunde liegenden pathophysiologischen Mechanismen sind bisher noch nicht genau erforscht und HDACi wurden noch nicht am humanen Myokard getestet. Des Weiteren können nicht-spezifische pan-HDACi schwerwiegenden unerwünschten Wirkungen, wie Myelosuppression führen, weshalb sie für die Therapie der HF nicht geeignet sind. Daher ist die Entwicklung Isoform-selektiver HDACi, notwendig.

Ziel:

In dieser Arbeit wurden Auswirkungen selektiver-HDACi auf humanes Myokard erstmals untersucht.

Methodik:

Dafür wurden atriale Trabekel vom rechten Herzohr unter dem Mikroskop isoliert und in eine spezielle Anlage überführt. Dabei wurden die Trabekel mit einer elektrischen Quelle, sowie mit einem Kraftmesser verbunden. Die Trabekel wurden anschließend mit Calcium-Ionen (Ca^{2+}) versetzt, mit einer fixen Frequenz von 1 Hertz (Hz) elektrisch stimuliert und bis zu einer optimalen Länge vorgedehnt. Dann wurden die Trabekel entweder mit einem der beiden selektiven HDACi, einem pan-HDACi oder mit Placebo für 2 Stunden inkubiert. Funktionelle Parameter wie systolische und diastolische Kraft und Bewegungsmechanik wurden kontinuierlich aufgezeichnet und analysiert.

Schlussfolgerung:

Die selektiven HDACi führten zu einem signifikanten Anstieg der entfalteten Kraft ohne Änderung der diastolischen Spannung im Vergleich zur Kontrollgruppe. Des Weiteren war die systolische und diastolische Kinetik der Trabekel (dp/dt_{max} und dp/dt_{min}), die mit den selektiven HDACi inkubiert wurden, signifikant schneller.

Zusammenfassend führten isoform-selektive HDACi zu einer Verbesserung der systolischen und diastolischen Parameter.

HDACi, die auf spezifische Isoformen wirken, beeinflussen direkt die diastolische und systolische Funktion. Daher sind sie eine hoffnungsvolle therapeutische Möglichkeit in der Behandlung von Patienten mit Herzinsuffizienz unabhängig der Ejektionsfraktion.

Abstract

Background:

Heart failure (HF) is a major public health issue and is combined with high morbidity and mortality. In Europe, 14 million patients living with HF. In Austria 1-2% of the adult population suffers from chronic HF, and almost 14,000 patients die of this every year. HF with preserved ejection fraction (HFpEF) represents about 50% of all HF cases. Typical features of HFpEF are left ventricular hypertrophy (LVH), elevated left ventricular end-diastolic pressure (LVEDP), left atrial enlargement, and elevated NT-proBNP plasma levels, despite a persevered left ventricular ejection fraction. These alterations result in impaired exercise capacity, fatigue, dyspnea, and edema. While there are several pharmacological strategies for treating heart failure with reduced ejection fraction (HFrEF) there are no detected effective therapies to improve outcomes in HFpEF, except for the use of sodium–glucose cotransporter 2 (SGLT-2) inhibitors. Thus, there is an unmet clinical need to develop new therapeutic options.

Histone deacetylases (HDAC) are enzymes that play an important role in controlling gene expression via posttranslational modification. HDAC inhibitors (HDACi) are clinically used for treating t-cell lymphoma. In preclinical studies the use of HDACi revealed positive effects related to myofibril relaxation. (1) However, the underlying pathophysiological mechanisms remain poorly understood, and HDACi has never been tested in human myocardium. Furthermore, non-specific, pan-HDAC inhibition can cause adverse effects such as myelosuppression, limiting its use in clinical practice. Thus, novel isoform-selective HDACi may be effective and reduce adverse effects.

Aim:

The aim of this research was to assess the effects of isoform-selective HDACi on human myocardium.

Methods:

Human atrial trabeculae were isolated from right appendages with microsurgical instruments. Then trabeculae were transferred into an organ bath, fixed with hooks and connected to an electric stimulator and a force transducer. Afterward, Ca^{2+} was added, and the trabeculae were electrically stimulated at 1 Hz. Subsequently, the

trabeculae were stretched to a length with the best strain. Finally, the trabeculae were incubated with two different isoform-selective HDACi or a pan-HDACi for 2 hours. Untreated trabeculae served as a control. Functional parameters like systolic and diastolic force, as well as twitch kinetics were continuously recorded and analyzed.

Conclusion:

The use of selective HDACi led to a significant, acute increase in developed force without altering diastolic tension compared with the control group. Furthermore, the selective HDACi increased systolic and diastolic kinetic parameters, reflected in an improvement of dp/dtmax and dp/dtmin.

In conclusion, isoform-selective HDACi increased systolic and diastolic functional parameters in human atrial myocardium. Therefore, isoform-selective HDAC inhibition, that enable the direct control diastolic and systolic function, may be a promising therapeutic option for treating patients with HF across the entire spectrum of the ejection fraction.

1. INTRODUCTION

1.1 What is epigenetic modification?

All somatic cells of the human body have an identical genome. Gene expression patterns determine the specific configuration and function of these cells in different organ systems. The principle of altering the gene expression involves modifications based on changes to the DNA (Deoxyribonucleic acid) and histone proteins without alteration of the base pairs. DNA methylation, histone alterations, and chromatin remodeling are the critical processes of epigenetic modification. Moreover, the effects of deviations in gene expression result in an increased risk of disease and changes in stress response. (2, 3)

1.1.1 Histone Modification

DNA is densely packed as chromatin in the cell nucleus by a spiral enwinding around nucleosomes. A nucleosome is a unit of a histone complex consisting of the four core histones (H3, H4, H2A, H2B) ordered by an octamer. Each of these nucleosomes includes 147 base pairs. (4) The linker histone H1 stabilizes the entire octamer complex, binding to the entry and exit of the DNA of the nucleosome. (5) Posttranslational modifications of the core histones are a crucial step in conformational chromatin changes, altering the gene expression by influencing DNA accessibility or obtaining diverse regulatory molecules. (6) An essential type of posttranslational modification is histone acetylation and deacetylation. Both processes occur at the lysin residues of the histone proteins. (7) Modifying the amino-terminal of the lysin residues induces synergistic and antagonistic interactions as well as dynamic alternations between the chromatin scaffold's transcriptionally active and silent states. (8) Acetylation, respectively, deacetylation of lysine, is a dynamic process controlled by two types of opposing enzymes, histone acetyltransferase (HATs) and histone deacetylases (HDACs). HATs, in touch with the cofactor acetyl coenzyme A (acetyl-CoA), effectuate the accumulation of an acetyl group to the ε-amino group of lysine. This transmission displaces the lysine residue's positive charge and further attenuates the connection between histones and DNA. In contrast to HATs, HDACs reverse the

acetylation and remove the acetyl group from the lysine residue. Consequently, the lysine residue regains the positive charge, and the chromatin scaffold will be stabilized, thereby limiting the gene expression. This process is required for gene expression, see Figure 1 for an overview of the process. (9, 10)

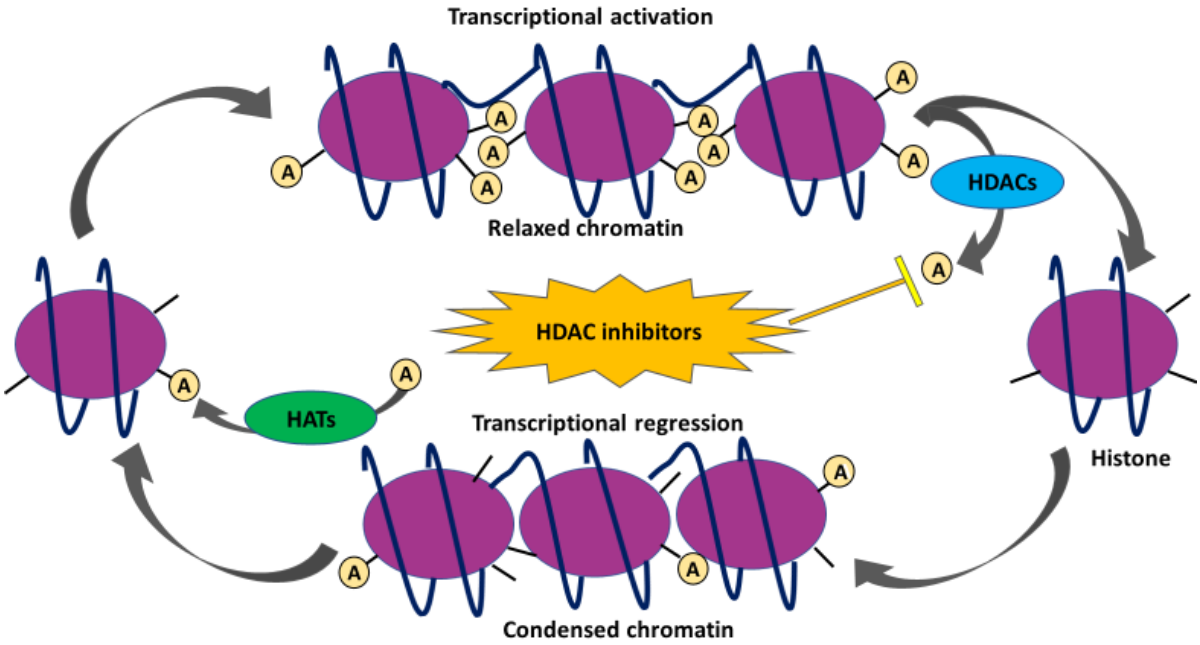

Fig. 1: Illustration of histone acetylation and deacetylation, the influence on chromatin structure, and starting point of HDAC inhibitors adapted from Chuang DM et al. HDAC inhibitors prevent the removal of an acetyl group from the ε-amino group of lysine. Thus, the chromatin structure remains slack, and gene transcription proceeds. (11)

Overall, HDACs are separated into four classes. Class 1 HDACs are composed of HDACs 1, 2, 3, and 8, and these are made up of a catalytic region consisting of an amino radical (NH_2) terminus and a carboxylic acid (COOH) terminus. Class 2 HDACs are subdivided into Class 2a (HDAC 4, 5, 7, and 9) and Class 2b (HDAC 6, 10). (12) Class 3 HDACs consist of sirtuins (SIRT 1-7), a species of nicotinamide adenine dinucleotide (NAD+) - dependent deacetylases (13), and Class 4 of the single-member HDAC 11. (12)

1.1.2 Epigenetic modifications in cardiovascular diseases

The two conditions of diluting and stabilizing the chromatin structure induce a transcriptional co-activation or repression (14, 15). It has been revealed that these processes are essential in normal physiology, and in the pathophysiology of

several diseases, including inflammation and heart failure. Studies have also exposed the indispensable role of HATs and HDACs in inadequate cardiac remodeling. (16) Furthermore, it has been demonstrated that Class 1 and Class 2 HDACs are decisive for the arrangement of cardiac hypertrophy. (17) It is assumed that cardiovascular diseases are associated with a dysregulation of post-transcriptional histone alterations. Furthermore, histone acetylation and deacetylation also represent a decisive role in regulating heart failure, hypertension, coronary artery disease, and pulmonary hypertension. Newer data has exposed that acetylation of histones attenuates several cellular mechanisms of cardiovascular diseases, such as inflammation, fibrosis, hypertrophy of cardiac myocytes, and apoptosis. Thus, the effects of HDAC inhibition on inflammation and cardiac remodeling in heart failure models were analyzed in recent investigations. (7)

An animal experiment on hypertensive rats treated with an HDAC inhibitor revealed an extenuated expression of inflammatory factors in the ventricle. The reduced spread of the inflammatory mediators decreased cardiac fibrosis and hypertrophy, subsequently improving cardiac function. (18) In another study performed on rodents, where chromatin immunoprecipitation was examined, it was revealed that the aggregation of HDAC1 induces apoptosis of cardiomyocytes in those animals. (19)

Generally, in various studies it was exposed that class I HDACs and class 2 HDACs are closely related to cardiac hypertrophy. It can be expected that class 1 HDACs extenuate antihypertrophic pathways, such as changing the Phosphoinositide 3-kinase/ Protein kinase B/ Glycogen synthase kinase-3 pathway (PI3K/Akt/Gsk3β pathway) through HDAC 2, thereby causing cardiac hypertrophy. (20, 21) In addition, it could be identified that HDAC 3 is associated with regulating cardiac outflow tract development in mice. (22) HDAC 8 and HDAC 6 activities also participate in cardiac fibrosis and hypertrophy, as demonstrated in chronic hypertensive rats. (23) However, the precise mechanism is still unclear. In diverse studies it has been suggested that Class I and class II inhibitors influence the regulation of cardiac hypertrophy contrarily. (24) Overall, all these studies involve effects related to different pathways caused by various classes of HDACs, which in turn regulate cardiac remodelling. (7)

1.2 The clinical use of HDAC inhibitors

The findings outlined in the previous sections lead to the theories that HDAC inhibitors can play a therapeutic role in cardiovascular diseases. (25) So far, HDACi were only used at the clinic for several types of cancer. HDACi once formed a new category of cytostatic therapy, these affect the activity of HDACs and have paved their way into oncological treatment algorithms. Subsequently, researchers discovered that this epigenetic mechanism regulates gene expression, affecting the cause and progression of diseases like lymphoma, myeloma, leukaemia, and lung cancer. Furthermore, it has also been revealed that altering the activity of HDACs leads to favourable effects on cell proliferation, migration, immune modulation, angiogenesis, and apoptosis. (26)
In 2006, the Food and Drug Administration (FDA) approved the HDAC inhibitor Vorinostat for treating cutaneous manifestations in people with T-cell lymphoma. Since then, the treatment of numerous malignant diseases with HDACi has been evaluated. (27, 28) Currently, just four HDACi have been authorized by the FDA for clinical use (26): Vorinostat, Belinostat (approved in 2014), Panobinostat (authorized in 2015), and Romidepsin (licensed in 2021). (29). In ongoing studies there is the aim to reveal whether this group of cytostatic agents also has positive outcomes regarding other kinds of cancer and non-malignant illness.(30-33) In the papers, it has been reported that HDAC inhibition is associated with a favourable result in inflammation disorders, and cardiovascular and neurodegenerative diseases. Based on these findings and the previously described findings in different animal models, new isoform-selective HDACi could positively affect the treatment of several cardiovascular disorders, including cardiac remodeling and fibrosis, hypertension, hypertrophy, and HFpEF. (34)

1.3 Epigenetic Regulation in Heart Failure

The pathophysiological processes of functional cardiovascular disorders are based on various epigenetic transformations in posttranslational modifications, such as DNA methylation, histone acetylation, and deacetylation, as described above. (35) In studies it has been revealed that the heart reacts to pathological stress with cardiac remodeling associated with cardiomyocyte hypertrophy, death, tissue inflammation, and fibrosis, followed by decreased cardiac function and heart

failure. Histone deacetylation plays a crucial role in cardiac fibrosis and remodelling, inducing the processes of impaired myocardial relaxation, diastolic function, myocyte contractility, and cell metabolism. (36) In studies with rats and mice it has been demonstrated that diastolic dysfunction can be enhanced by exponentiating myofibril relaxation through the inhibition of histone deacetylation. (37) However, these experiments were restricted through the small size of the animals and the differential physiological functions compared to large animals, which have a similar pathophysiological mechanism in heart failure to humans. (38) In a large mammalian study, it has been revealed that inhibition of histone deacetylation by HDACi leads to a curtailing of the advancement of hypertrophy of the left ventricle combined with a decrease in wall thickness. Furthermore, the elevated LA size due to HFpEF began to reduce. Another consequence of HDAC inhibition was the extenuation of an increased indicator of left ventricular diastolic function (É/e), thereby suggesting degraded left ventricular filling pressures. É/e is used in clinical research and clinically to evaluate left ventricular filling pressure and diastolic function. (39) Felines medicated with the HDAC inhibitor suberoylanilide hydroxamic acid (SAHA) showed improved inotropic supply compared to the control group in a stress test with dobutamine. In addition, in this study it was shown that HDAC inhibition significantly decreased LVEDP compared to the control group. These findings suggest that the inhibition of histone deacetylation enhances systolic and diastolic function in banded animals. In the following course of this research, samples of myofibrils from the left ventricle were isolated, and mechanical studies were executed. The results revealed that inhibition of HDACs leads to enhanced myofibril relaxation. These findings show that HDAC inhibition leads to strong antihypertrophic effects (LV wall thickness and LA size) in the animals of this study. Moreover, it has been revealed that the treated animals have enhanced LV systolic and diastolic function. (1)

1.4 HDAC Inhibitors in heart failure – a gap in the evidence

The previous effective therapy options used for HFpEF are few in number, where it was focus was placed on treating HFpEF-associated symptoms and conditions like reducing volume overload by diuretics and hypertonic blood pressure through angiotensin converting enzyme inhibitors (ACE inhibitors), angiotensin II receptor

blockers (ARBs), calcium antagonists, and beta-blockers. In several randomized clinical trials there was a failure to show any clear benefits of these drugs in patients with HFpEF. However, the FDA has recommended the use of Spironolactone and Sacubitril/Valsartan for treating patients with an LV ejection fraction "less than normal". The decision to use sacubitril/valsartan was predicated on the basis of various meta-analysis about the prospective comparison of the angiotensin receptor/neprilysin inhibitor (ARNI) with ACE inhibitors. This analysis was done in order to discover the impact on global mortality and morbidity in HF (PARADIGM-HF) and about the prospective comparison of ARNI with ARBs in global outcomes in HFpEF (PARAGON-HF). Moreover, a subgroup analysis from the PARAGON-HF trial was use for the decision. In the studies a decrease was demonstrated in heart failure hospitalizations and cardiovascular death in patients with an ejection fraction down the normal scope. Likewise, Spironolactone has shown a significant lowering in cardiovascular death and hospitalizations. (40) "*The Empagliflozin Outcome Trial in Patients with Chronic Heart Failure with Preserved Ejection Fraction (EMPEROR-preserved)*" (41) and "*the trial testing of Dapagliflozin in HFpEF and mildly reduced ejection fraction (DELIVER)"* (42) involved the analysis of the effects of SGLT2-inhibitors in patients with HF and an EF over 40%. They published their results in the New England journal of Medicine in 2021 and 2022. (41, 42) The results of the EMPREROR-preserved trial revealed that "*Empagliflozin reduced the combined risk of cardiovascular death or hospitalization for heart failure in patients with heart failure and a preserved ejection fraction, regardless of the presence or absence of diabetes.*" (41) In the DELIVER trial it was disclosed that *"Dapagliflozin reduced the combined risk of worsening heart failure or cardiovascular death among patients with heart failure and a mildly reduced or preserved ejection fraction."* (42). Last year, the "2022 AHA/ACC/HFSA Guideline for the Management of Heart Failure" (43) classified the SGLT2 inhibitor as a 2a recommendation in the treatment of HFpEF. The justification of the classification is, *"In patients with HFpEF, SGLT2i can be beneficial in decreasing HF hospitalizations and cardiovascular mortality."* (43) Indeed, the prognosis of cardiovascular and HF deaths is better in HFpEF than in HFrEF, but the difference in mortality rates was insignificant (44). In contrast, the rate of non-cardiovascular deaths is higher in HFpEF than in HFrEF. It has been shown that also the prevalence of HFpEF increases over time compared to the

prevalence of HFrEF. (45) Consequently, while there are many therapeutic options in treating HFrEF, the treatment of HFpEF is limited. Thus, therapeutic options for the treatment of HFpEF is an unmet clinical need.

Inhibition of histone deacetylation was found to cause a variety of positive effects in small and large animal models mimicking a HFpEF phenotype. The currently available and approved HDAC inhibitors are associated with adverse effects which limits their use. Therefore, specific HDAC inhibitors which can modulate cardiac function have to be developed and tested in human cardiac tissue and cells. This field of research could enable new therapeutic options for treating patients with HFpEF in the future.

2. Heart Failure

2.1 Definition of heart failure

"According to the new guidelines for the diagnosis and treatment of acute and chronic heart failure from the ESC, heart failure is not a single pathological diagnosis, but a clinical syndrome consisting of cardinal symptoms (e.g. breathlessness, ankle swelling, and fatigue) that may be accompanied by certain signs (e.g. elevated jugular venous pressure, pulmonary crackles, and peripheral oedema). It is due to a structural and/or functional abnormality of the heart that results in elevated intracardiac pressures and/or inadequate cardiac output at rest and/or during exercise." (40)

This syndrome is divided into four groups, classified by the ejection fraction of the left ventricle. A symptomatic HF with a LVEF ≤ 40% is considered as a HFrEF, and a symptomatic HF with a LVEF of 41 to 49% is regarded as a HFmrEF. A symptomatic HF with a LVEF ≥50% is considered as a HFpEF. The fourth group is called HF with improved ejection fraction (HFimpEF) and is defined through symptomatic HF with a baseline LVEF ≤40%, a ≥10 point rise from baseline LVEF, and a repeated measurement of LVEF >40%. (46)

While plenty of therapeutic options for the treatment of HFrEF are available (47-51), these agents showed poor results in conditions of HFmrEF or HFpEF (52, 53). However, in retrospective studies, it has been indicated that patients with ejections fractions from 40-50% may benefit from similar treatments to those used for HFrEF. Based on these facts, HFmrEF is defined separately from HFpEF because this subgroup's current therapeutic options are inefficient. (40, 54)

2.2 Heart Failure with preserved Ejection Fraction

HFpEF is a cardiovascular syndrome with an ejection fraction >50% and is associated with limited quality of life, increased hospitalizations, poor prognosis, and elevated mortality. (55)

2.2.1 Risk factors of HFpEF

In several studies the risk factors leading to increased incidence of HFpEF have been analysed and it was reported that women have HFpEF and older people more often. For example, in the Olmsted County, Minnesota study it has been revealed that patients with incident HFpEF were older than patients with HFrEF. This age-related risk has also been observed in other studies. (56, 57) In other studies it has been indicated that atrial fibrillation, chronic kidney disease, and non-cardiovascular comorbidities such as obesity, as it is estimated that more than 80% of patients are overweight, diabetes mellitus, and hypertension were indicated more often in patients with HFpEF than in patients with HFrEF. (58, 59)

2.2.2 Pathogenesis and the influence of diastolic dysfunction on HFpEF

The risk factors demonstrated above, like obesity, hypertension, diabetes, additional dyslipidemia, and metabolic syndrome, induce systemic inflammation through various inflammation mediators. Oxidative stress causes structural and cellular adjustment of the heart, and endothelial inflammation and dysfunction, through diverse, complex pathophysiological processes. (60) Many patients diagnosed with HFpEF have a concentric hypertrophic remodeling of the left ventricle through increased afterload, denoted by average or almost normal end-diastolic volume, expanded wall thickness, expanded myocardial mass to hollow volume, and augmented relative wall size. (61) Diastolic dysfunction also increases the risk of generating HFpEF, which means that diastolic dysfunction and HFpEF are not synonymous terms, but diastolic function can be part of it. The active pressure drops in the early diastole correlate to calcium reuptake. Myofilament relaxation describes the diastolic function. (62) Functional abnormalities of the relaxation during the diastolic phase, the elasticity of the left ventricle, and filling of the ventricle, despite normal or abnormal LV ejection fraction and regardless of the patient, either show symptoms or do not describe the diastolic dysfunction. Furthermore, the pressure fall ratio in the isovolumetric relaxation stage is extended in HFpEF. (37) The left ventricle improves relaxation, permitting quicker pressure drop when the heart rate rises, but in HFpEF, this process is impaired. Studies have exhibited that diastolic dysfunction caused no

impairment of the net LV filling, but abnormally elevated pressure is required for a sufficient filling. (61) Despite a normal or nearly normal ejection fraction in patients with HFpEF, in studies it has been indicated that those patients also have limited improvement of systolic function, especially during exercise. The reduced systolic reserve minimizes cardiac output as well as end-organ perfusion. (62) Moreover, the ventricular stiffness and the slowed relaxation result in elevated left ventricular filling pressures, inducing increased pressures in the left atrium and enlargement and remodeling of the atrium over time. The LA's high pressure can lead to dyspnoea and secondary pulmonary hypertension, continuative developing right ventricular dysfunction, and atrial fibrillation. (63)

2.2.3 Diagnostic of HFpEF

Two helpful score-based algorithms exist, H_2FPEF (Tab.2) and HFA-PEFF (Fig.2), for the assessment of HFpEF. These algorithms have been tested in various studies. However, the implementation, as well as the sensitivity and specificity, was not always the same. For clinical application, the algorithms were simplified and included significant elements which are widely available to clinicians. The simplified procedure begins with an evaluation of the pre-test possibility, including signs of heart failure, an ejection fraction >50%, objective evidence of abnormalities in the cardiac structure and/or function, combined with left ventricular diastolic function and/or increased filling pressures, and clinical characteristics like LA size (>34 mL/m^2) and E/é ratio >9. (40)

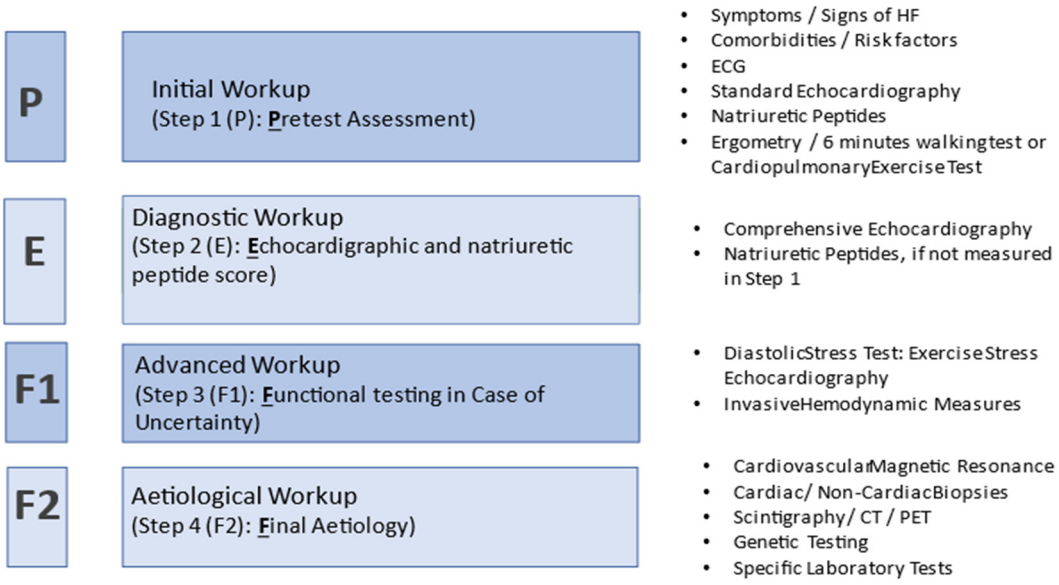

Fig. 2: Scheme of the diagnostic tool HFA-PEF used to assess HFpEF based on symptoms, risk factors, clinical measurements, laboratory chemistry tests and non-invasive or invasive imaging, and measurements. (64)

	Clinical Variable	Values	Points
H_2	Heavy	Body mass index > 30 kg/m^2	2
	Hypertensive	2 or more antihypertensive medicine	1
F	Atrial Fibrillation	Paroxysmal or Persistent	3
P	Pulmonary Hypertension	Doppler Echocardiographic estimated Pulmonary Artery Pressure > 35 mmHg	1
E	Elder	Age > 60 years	1
F	Filling Pressure	Doppler Echocardiographic E/é > 9	1
	H_2FPEF-Score		Sum (0-9)

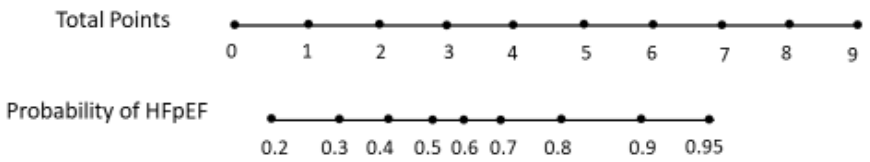

Tab. 1: Diagnostic tool H_2FPEF used to estimate the probability of HFpEF on the basis of clinical variables and determined values (65)

2.3 Scope of the Problem

HF is a significant healthcare issue with all its presentation. In Austria, around 1-2 % of the adult population suffer from heart failure, and nearly 14,000 patients die every year because of HF. In Europe, there are 14 million patients with HF, and in 2020 nearly 64 million people lived with HF worldwide. In studies it has been suggested that the age-adjusted incidence of HF is attenuated and seems to decrease. In contrast to the incidence, the prevalence of HF is growing. From data the prevalence is estimated at 1% to 2% of the adult population. The consequences of this can be fatal. About 20-30 % of diagnosed patients die within one year. Almost 50% of HF patients die within five years after obtaining a diagnosis. (66-69) Nearly half of the HF patients have HFpEF and the age-adjusted incidence and prevalence are rising. (57, 70) The increasing number of patients with HFpEF is a major public health problem and one of the greatest challenges in modern medicine with a significant financial burden. During cost-of-

illness studies, it has been demonstrated that the annual prevalence-based expenses for a patient with heart failure amount to $25,532 for Germany. The lifetime expenditures for these patients come to $126,819. (71) Therefore, HFpEF is a substantial healthcare problem as this disease accounts for about half of the patients diagnosed with HF without effective treatments, apart from the recently discovered effects of the $SGLT_2$ inhibitor empagliflozin. (72, 73)

2.4 Physiology of cardiac function

To understand the involved processes leading to impaired HF, knowledge of the physiological heart mechanics, especially the excitation-contraction coupling, is essential.

2.4.1 The action potential

The heartbeat is a rhythmic electromechanical cycle of contraction and relaxation followed by a time of refractoriness. The electric function depends on the sequential activation of cells in focused pacemaker zones of the heart. Myocardial action potentials result from ion channels' activation and inactivation, leading to different intracellular and extracellular sodium, calcium, and potassium concentrations. (74) The Na^+ influx in specialized pacemaker cells at the sinoatrial node (SA) leads to a spontaneous depolarization via the opening of hyperpolarizing-activated cyclic nucleotide-gated (HCN) channels. Moreover, intracellular Ca^{2+} cycling has been suggested to operate as a primary controller of SA node depolarization. (75) Spontaneous Ca^{2+} signals developed from the sarcoplasmic reticulum (SR) reach the SA node and are called Ca^{2+} sparks. Ca^{2+} sparks mobilize sodium/calcium exchange, at which 3 sodium ions (Na^+ ions) enter the cell for every leaving Ca^{2+} ion. This transposition assists membrane depolarization. The resting membrane potential, around -70 millivolt (mV), increases through depolarization until it reaches a critical swell value (-40 to -50 mV). L-type (long-lasting, regarding the length of activation) Ca^{2+} channels at the plasma membrane are opened by overshooting the threshold. This process permits a large influx of Ca^{2+} ions into the myocytes' cytosol, boosting the membrane potential to +10 mV. During the Ca^{2+} influx, also voltage-dependent

Potassium ion (K^+) channels start to open. Thus, K^+ ions flow out of the cell. This process represents the repolarization of the myocytes. During this process, the membrane potential decreases to the initial value. This value equates to the maximum diastolic potential. Subsequently, the sodium/potassium-ATPase (N^+/K^+-ATPase) and the sodium/calcium exchanger (NCX) restore the primary extracellular and intracellular ion concentrations. The depolarization signal spreads from the SA node through the cardiac conduction system. The electrical linkage between cells through gap junctions is essential for this transmission. The transmitted action potential on the other fields of the myocardium varies in regard to a few steps from the action potential of the pacemaker cells. Voltage-dependent Na^+ channels permit an intense Na^+ influx at the beginning of the stimulus. This influx leads to a rapid increase in the potential. Subsequently, the Ca^{2+} influx starts via L-type voltage-operated Ca^{2+} channels (VOCCs), eventually developing a plateau and elongating the action potential duration. This process elevates the absolute refractory period and prevents circulating excitation. (74, 76) These transmitted electrical potentials provoke mechanical contraction of the heart through an intracellular calcium-dependent process known as excitation-contraction coupling (ECC) (77)

2.4.2 The excitation-contraction coupling

The excitation-contraction coupling delineates a chain reaction consisting of depolarization of the myocyte membrane via action potential, ion channel activation on the surface of the membrane, and calcium discharge from the sarcoplasmic reticulum. These procedures require an enormous amount of cellular energy. Most of this energy is provided by mitochondria. The energy production cycle begins with the transformation of glucose to pyruvate, which enters the mitochondria. In these, pyruvate dehydrogenase (PDH) converts pyruvate to acetyl-CoA. In addition, fatty acyl-CoA, converted from fatty acids, moves from the cytosol to the mitochondria. Through ß-oxidation of acyl-CoA the main end-products acetyl-CoA, nicotinamide adenine dinucleotide + hydrogen (NADH) and the reduced form of flavin adenine dinucleotide ($FADH_2$) are generated. Acetyl-CoA from both ß-oxidation and glycolysis ends up in the tricarboxylic acid (TCA) cycle. During the course of this cycle, Acetyl-CoA is transformed into NADH and

$FADH_2$. NADH provides the respiratory chain with electrons. During consecutive redox reactions, protons are relocated at the intermembrane space thereby establishing a proton gradient and an electrical gradient (Δψm) across the inner membrane of the mitochondria. This gradient creates a proton motive force. The electrons that move through the respiratory chain are converted to oxygen (O_2) and eventually to water (H_2O). At the last respiratory chain complex, the proton motive force supplies the required energy to transmute adenosine diphosphate (ADP) to adenosine triphosphate (ATP). This process is known as oxidative phosphorylation. The crucial regulators of oxidative phosphorylation are ADP, phosphate (P_i), and Ca^{2+}. During the action potential, Na^+ flows inwardly via voltage-gated Na^+-channels (I_{Na}) and so causes a rapid polarisation of the cell membrane (~-90 mV to ~+20 mV). Due to the membrane depolarization, L-type voltage-gated Ca^{2+} channels on the surface of the membrane open, and Ca^{2+} streams into the myocytes. The Ca^{2+}-Influx via voltage-gated Ca^{2+}-channels (I_{Ca}) initiates Ca^{2+} emission from SR through the ryanodine receptor (RyR), a ligand-gated Ca^{2+} channel. This sequence is identified as Ca^{2+} induced Ca^{2+} release (CICR). Increased Ca^{2+} concentration in the myocyte cytosol activates contractile units resulting in cardiac contraction. Afterward, the SR Ca^{2+}-ATPase (SERCA) pumps the Ca^{2+} reverse to the SR and restocks the Ca^{2+} store. Furthermore, the NCX replaces intracellular Ca^{2+} with Na^+. (76, 78, 79)

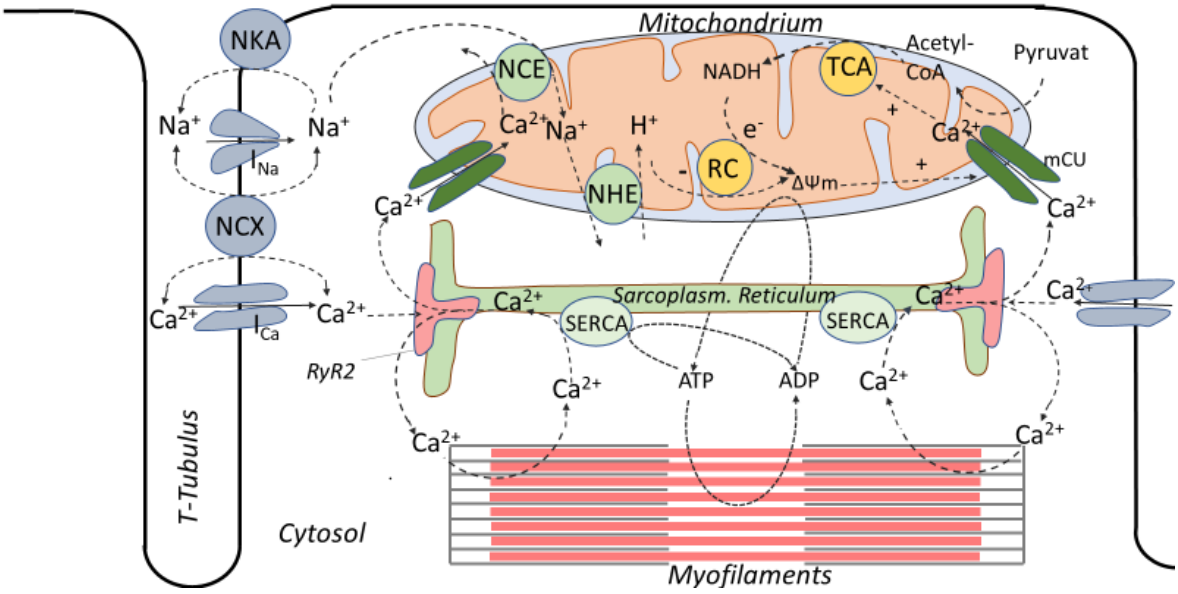

Fig. 3: Overview of excitation-contraction coupling in cardiac myocyte and mitochondrial energy production from Maack C. and O'Rourke B. SERCA: SR Ca2+ ATPase; TCA: tricarboxylic acid

cycle; RC: respiratory chain; Δψm: mitochondrial membrane potential; NCE: mitochondrial Na+/Ca2+-exchanger; NHE: mitochondrial Na+/H+ -exchanger; NKA: Na+/K+-ATPase; NCX: Na+/Ca2+-exchanger; RyR2: ryanodine receptor type 2; mCU: mitochondrial Ca2+-uniporter; I_{Na} and I_{Ca}: voltage-gated Na+- and Ca2+-channels (79)

2.4.3 Contraction and Relaxation

As seen in the previous section, Ca^{2+} plays an essential role in the formation of cardiac contraction. A transformation of the conformation of the protein myosin, binding on actin filaments, triggers the myocyte's contraction. The process of contraction is ATP-dependent. In the resting state, Tropomyosin encloses the actin filament and inhibits the binding sites of myosin. Troponin C binds four Ca^{2+} ions from the released Ca^{2+} ions from the SR during the action potential. Thus, the Troponin-Tropomyosin-complex alters its conformation, and myosin can bind at actin via cross-bridges binding. The strongly bounded myosin traverses move into the actin filaments. The actin filaments glide into the myosin. Thereby the length of the actin-myosin complex is shortened. The correlation between Ca^{2+} release during the action potential and the interaction between myosin and actin filaments is known as electromechanical coupling. At the end of the contraction, ADP dissolves from the myosin head. Then, a new ATP can bind, and a further contraction cycle will start. Concomitant to this, SERCA, and NCX decrease cytosolic Ca^{2+} concentration during the diastole. Thus, the bounded Ca^{2+} is detached from Troponin C. Tropomyosin then inhibits the binding site of myosin on the actin filaments again. Consequently, the muscle relaxes. (80-82)

2.5 Aim of the study

The aim of this study was to investigate the effects of a pan- and two different non-commercially available isoform-selective HDACi in human atrial tissue compared to a control group. HDACi has never been previously tested on human myocardium. The current work was focused on the effects of HDACi on functional cardiac properties in atrial human trabeculae.

3. MATERIALS AND METHODS

The experiments for this work were based on samples from the right atrial tissue of the human heart. In sum, tissues from 13 different patients were used. All these patients gave informed consent before their cardiac surgery. This study was approved by the Ethics Commission of the Medical University of Graz.

3.1 Acquisition of Atrial Tissue

The tissue samples were obtained during heart surgery. Routine cardiac surgery requires an immobile heart, therefore interventions like coronary artery bypass graft surgery or heart valve replacement / repair are performed with the help of a heart-lung machine to maintain blood circulation through extracorporeal circulation. The venous connection occurs through cannulation of the right atrium. During this procedure, the surgeon displaces the right atrial appendage. The removed atrial appendage's average size was about 2 x 1 x 0.5 centimetres (length x width x depth).

3.2 Buffer Solutions

The removed atrial appendage tissue was not exposed to autolytical processes, so the tissue had to be transferred in a buffer solution, respectively nutrient solution. This solution used consisted of a unique buffer solution, the “Tyrode´s solution (Tab. 3)," and added 2,3-butanedione monoxime (BDM). BDM is a myosin ATPase inhibitor that suppresses cardiac muscle contraction (83). A cardioplegic condition was achieved by inserting the tissue samples in the Tyrode´s solution with BDM. This state is necessary for tissue maintenance. Tyrode´s solution (without BDM) was used as a buffer and nutrient medium during all experiments.

Tyrode´s Solution	
Solid matter	**Mass (1L)**
NaCl	7.422 g
$NaHCO_3$	2.100 g
Glucose	2.018 g
KH_2PO_4	0.177 g
KCl	0.172 g
$MgSO_4 \cdot 7H_2O$	0.148 g
$CaCl_2 \cdot 2H2O$	0.029 g
Altinsulin	5 I.E.

BDM Solution	
Solid matter	**Mass (1L)**
NaCl	7.422 g
2,3-BDM	3.000 g
$NaHCO_3$	2.100 g
Glucose	2.018 g
KH_2PO_4	0.177 g
KCl	0.172 g
$MgSO_4 \cdot 7H_2O$	0.148 g
$CaCl_2 \cdot 2H2O$	0.029 g

Tab. 3: Composition of used buffer solutions.

3.3 Transport of Atrial Appendage

After the surgical removal of the right atrial appendage, the tissue was put straight into a cup filled with the solution of Tyrode and BDM. Afterwards, the atrial tissue was taken as quickly as possible to the lab. To support the maintenance of tissue vitality during transport, the BDM-Tyrode solution was aerated with carbogen before.

3.4 Preparation of Atrial Tissue

After transport to the lab, the atrial appendage was transferred carefully to a dissection tray filled with the BDM-Tyrode´s solution saturated with carbogen to preserve the cardioplegic condition. Then, the atrial appendage was surveyed under the microscope to look at the muscle strips inside and how they were located. The following step was to prepare the muscle strips with microsurgical tweezers and scissors in order to extract unbranched muscle strips. The muscle strips were prepared to be not too large because hypoxic processes may result and not too small because they do not match the experimental setup. The prepared, isolated muscle strips were moved with a pipette to a new carbonated cup filled with BDM-Tyrode´s solution and accumulated there for the subsequent experiment.

All preparation steps were performed atraumatically without too much stretching of the muscle strips and applied pressure because this could induce irreversible tissue damages.

3.5 Experimental Setup for Muscle Strip Experiments

All experiments for this work were performed using a unique measuring system, shown in Figure 4. The measuring system consists of the following:

- Measurement system with a force transducer and bridge amplifier
- Electrical stimulator
- Organ bath, two-chamber cuvette system with separated oxygenation
- Temperature controller
- Stereomicroscope
- Computer with software program LabChart Version 7 pro

The entire experimental construction was put together by “scientific instruments Heidelberg” in Germany.

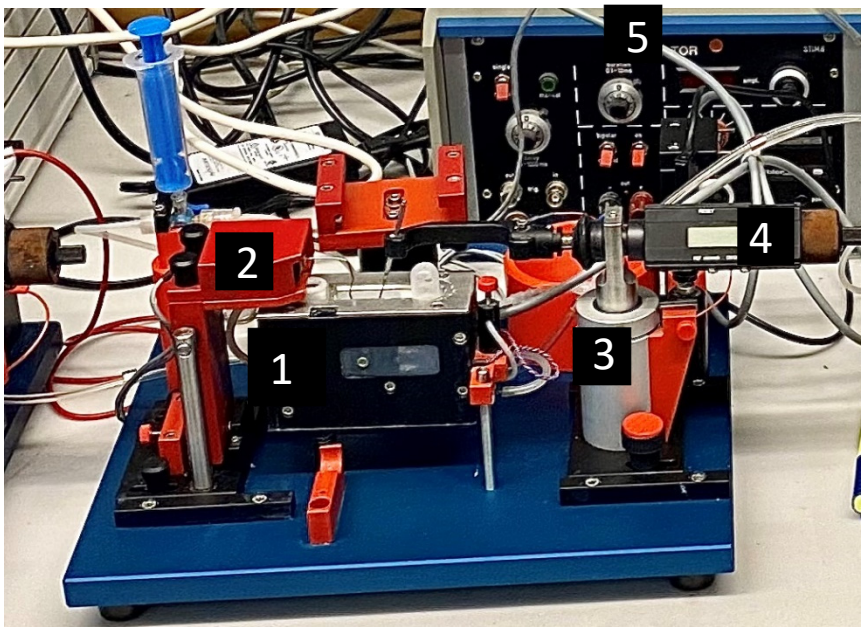

Fig. 4: Experimental Setup; 1: Organ bath, 2: Force transducer, 3: Electrical Stimulator, 4: Micrometre Screw, 5: Temperature controller

Fig. 5: Right atrial appendage

After the preparation, the muscle strips had to undergo a washout of the Tyrode-BDM solution to neutralize the cardioplegic condition. This procedure was essential for the subsequent electrical stimulation of the muscle strips because

otherwise, the muscle strips would not start contracting. The washout process contains three steps for the elimination of all residues of BDM in the tissue. The solution in the cups for washing this out is a Tyrode solution with glucose, and it is the same solution filled in the organ bath where the muscle strips were subsequently inserted. After this washout, the muscle strips were inserted carefully in the organ bath with tweezers below the microscope on small hooks.
The organ bath is part of a two-chamber cuvette system. One chamber, the organ bath, the central part of the setup, was filled with Tyrode´s solution and contains the muscle trabecula. The use of Tyrode´s solution guarantees the nutrient supply for the muscle strips. On the one hand, the second chamber is for permanent oxygenation in order to maintain the pH value in physiological conditions. On the other hand, for the oxygen supply for the trabecula. A tiny screw adjacent to the organ bath was used to regulate the intensity of gas influx. The gas influx and the ascending gas bubbles induced a flow in the two-chamber system, a permanent mixture. Thus, variability in the temperature and pH of the solution can be prevented. The temperature controller kept the organ bath temperature constant at 36°C because, at higher temperatures, the proteins would begin to denature, and lower temperatures would cause restrictions on the contractility of heart muscle cells. In addition, the solution flow avoids measurement disturbances due to the bubbles. (Fig. 6) In the place where the gas bubbles reach the surface, a transparent cap is located. Among other things, this cap averts the solution loss from the cuvette by bursting gas bubbles. The organ bath is the central part the muscle strip setup construction. The setup includes four channels with an organ bath, oxygenation, and temperature controller.

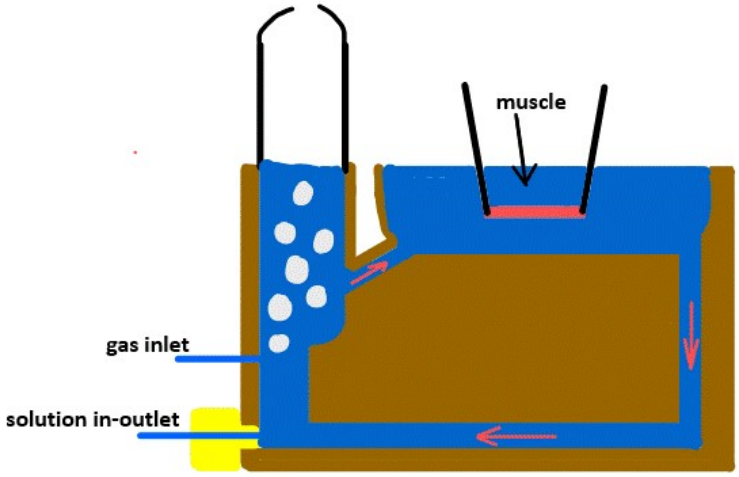

Fig. 6: Schema of the used organ bath and mounted muscle strip.

One of the two hooks, on which the atrial trabecula was hung, was connected with a force transducer, thereby making it possible to detect the contraction force. As a consequence, the muscle strip`s inotropy and lusitropy could be evaluated. The other hook was attached to a micrometre screw. With this screw, the trabecula were stretched to an ideal length between sarcomeres (L_{max}), thereby simulating the increasing preload, needed for achieving the most significant isometric contraction as part of the Frank-Starling-Mechanism. (84)

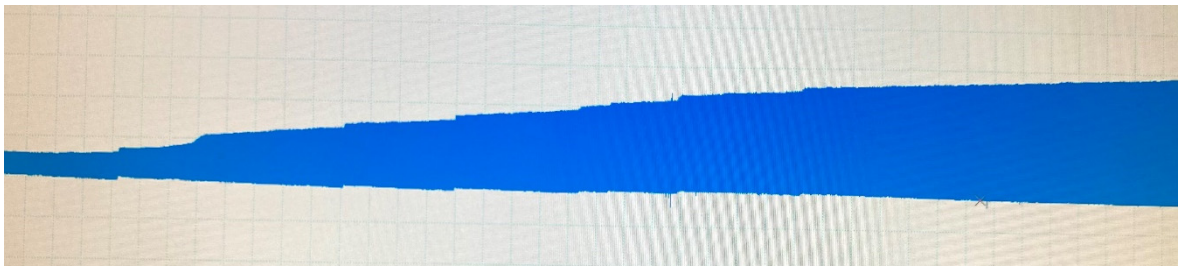

Fig. 7 Stretching steps of the muscle strip.

The state of the greatest contraction was the starting point for the following steps of the experiment. The electrical stimulation of the trabeculae resulted from a point stimulation from the electrical stimulator. This kind of stimulation occurs when the electrical stimulus transfers from cell to cell. Before the electrical stimulation started, the organ bath's nutrient solution was saturated to physiological Ca^{2+} concentration levels for the optimal contraction of the trabeculae. This procedure occurred in two steps so that the muscle strips had enough time for adaptation to the modified Ca^{2+} concentration. Afterwards, the trabecula was stretched through Lmax, as mentioned above, and the experiment could begin.

3.6 Substances

The active ingredients, two different selective HDACi, Rodin A and IRBM-D were acquired from ITALFARMACO, Italy. IRBM-D is a selective inhibitor of HDAC 1, 2 and 3. Rodin A interferes with HDAC 1 and 2. The third active ingredient, a pan-HDACi, Givinostat, was obtained from CHEMIE S.p.A, France. IRBM-D was utilized in a concentration of 250nM and Rodin A in a concentration of 2µM.

Givinostat was used at a concentration of 250nM. 2µM DMSO (Dimethylsulfoxide) was used for the control group.

3.7 Experimental Measurement Steps

In the experiments the effects of selective and non-selective HDAC inhibition on inotropy and lusitropy of the heart muscle tissue were analysed.

3.7.1 Single-dose Experiments

After diluting the agents with DMSO, the substances were added separately to an organ bath filled with nutrient solution, including the stretched (L_{max}) trabeculae. The compounds were pipetted to the solution as a single shot in a particular concentration, 250 nM Givinostat, 250 nM IRBM-D, and 10 µM Rodin A. Furthermore, the fourth experimental run was for a control test, performed with a single shot of DMSO, the solvent of the active ingredient. The control group with DMSO serves as a comparison for the effects of the HDACi. Moreover, the control test is essential because the stimulated trabeculae lose force over time during the trial duration regardless of the applied treatement
After pipetting the substances, the stimulated trabeculae were incubated for 120 minutes. The force development was recorded through the force transducer across this interval, and the measuring points were every 15 minutes.

3.7.2 Analysis

Within each experimental group, the muscle strips were prepared using the same conditions. The information, measured from the force transducer, was relayed to the measuring program LabChart on the computer. In particular, the developed force and relaxation time of the trabecula were investigated at the measurement points. Therefore, ten consecutive contractions showing similar movement were selected at the measuring point, and the average kinetic data were determined. The developed force was analyzed as a percent of BL, while diastolic tension was evaluated in terms of absolute values. To compare the impacts of developed force

after an intervention, changes were demonstrated as the delta of developed force. The delta of developed force is defined as the alteration in the relative data in terms of percent of BL. All results are depicted as the mean values ± standard error of the mean (SEM).

3.7.3 Statistics

Statistical analyses and data management were conducted using Graph Pad PRISM 7.05 (La Jolla, CA, USA). A repeated measure two-way ANOVA was used for the functional measurements in human trabeculae. For analyzing multiple comparisons via post-hoc tests, Dunnett's multiple comparisons test was utilized. It was evaluated if the values of one intervention group change with time compared to their baseline and if there were alterations between the three HDAC inhibitor groups compared to the control group. For all statistical tests, a double-sided test was performed. A p-value of ≤0.05 was utilized to appoint significance for all statistical measurements.

4. RESULTS

4.1 Demographic Data

In total trabeculae from 13 patients undergoing cardiac surgery were utilized for this study. The trabeculae had to meet specific criteria in order to be eligible for the study (no arrythmias, developed force > 5 mN/mm²), data from 13 patients were collected. The patients´ demographics are displayed in table 3.

For the IRBM-D group, personal information from nine of the patients were registered and for the Rodin A group information from eight of the patients were gathered. The control group involves data gathered from eight of the patients. The following data were investigated: age, sex, BMI, heart rhythm (sinus rhythm vs. atrial fibrillation), echocardiographic measured EF and importantly cardiovascular pre-existing conditions like aterial hypertension, diabetes mellitus, hyperlipidaemia, obesity (BMI > 30 kg/m^2) and active nicotine abuse. Furthermore, the relevant long-term medication was obtained. In addition, the type of surgical intervention like CABG or aortic valve replacement or a combination of both, in which the atrial appendages were obtained, were analyzed.

Parameter	Givinostat (n=7)	IRBM-D (n=9)	Rodin A (n=8)	DMSO (n=8)
Age - Years	73±10	67±10	70±9	68±9
Female - No. (%)	2 (29%)	1 (11%)	2 (25%)	1 (13%)
BMI - kg/m^2	26.5±3.8	25.6±4.8	25.6±4.8	28.7±0.4
Sinus Rhythm - No. (%)	5 (71%)	9 (100%)	7 (88%)	6 (75%)
Ejection Fraction ≥50% - No. (%)	7 (100%)	9 (100%)	8 (100%)	8 (100%)
Pre-existing Condition:				
Diabetes Mellitus - No. (%)	2 (29%)	2 (22%)	2 (25%)	2 (25%)
Smoker - No. (%)	2 (29%)	3 (33%)	3 (38%)	5 (63%)
Arterial hypertension - No. (%)	6 (86%)	6 (67%)	6 (75%)	6 (75%)
Obesity - No. (%)	0 (0%)	3 (33%)	3 (38%)	2 (25%)
Hyperlipidaemia - No. (%)	3 (43%)	4 (44%)	2 (25%)	2 (25%)
Medication:				
ACE-Inhibitor - No. (%)	4 (57%)	7 (78%)	5 (63%)	6 (75%)
ARB - No. (%)	1 (14%)	0 (0%)	1 (13%)	1 (13%)
Beta-blocker - No. (%)	7 (100%)	8 (89%)	7 (88%)	7 (88%)
Calcium-channel blocker	3 (43%)	2 (22%)	3 (38%)	2 (25%)
Mineral receptor agonists - No. (%)	1 (14%)	0 (0%)	1 (13%)	1 (13%)
Statin - No. (%)	5 (71%)	7 (78%)	7 (88%)	8 (100%)
Metformin - No. (%)	1 (14%)	2 (22%)	2 (25%)	1
GLP1-antagonist - No. (%)	0 (0%)	1 (11%)	0 (0%)	1 (13%)
Type of surgery:				
Coronary artery bypass grafting - No. (%)	5 (71%)	5 (56%)	4 (50%)	4 (50%)
Aortic Valve Replacement - No. (%)	2 (29%)	3 (33%)	3 (38%)	1 (13%)
CABG + Aortic Valve Replacement - No. (%)	1 (14%)	1 (11%)	1 (13%)	3 (38%)

Table 3. Demographic data

4.2 Functional effects on human atrial myocardium

The functional influence of HDAC inhibitors of the human atrial myocardium was compared to a control group. For this, suspended muscle strips were analysed with regard to different functional parameters. These parameters are systolic, diastolic, and developed force, dp/dt_{max}, dp/dt_{min}, RT 50%, and Tau.
The diastolic force is indicated the open-circuit voltage of the mounted muscle strips. The systolic force is described by the contractile force of the trabeculae. The collected data refers to the relative value of the starting point of the experiment (=100%).

4.3 Functional effects on systolic force

The influence of three different HDAC inhibitors on the inotropy of atrial tissue was measured. Trabeculae were gradually stretched until max. force was reached, which served as the baseline (100%) for subsequent experiments. After pipetting the agent into the organ bath, the force data were continuously recorded and analysed every 15 minutes. The systolic force describes the contraction power of the muscle strips. Both specific HDAC inhibitors IRBM-D and Rodin A caused an apparent increase in systolic force compared with the control group with DMSO and the pan-HDAC inhibitor Givinostat.

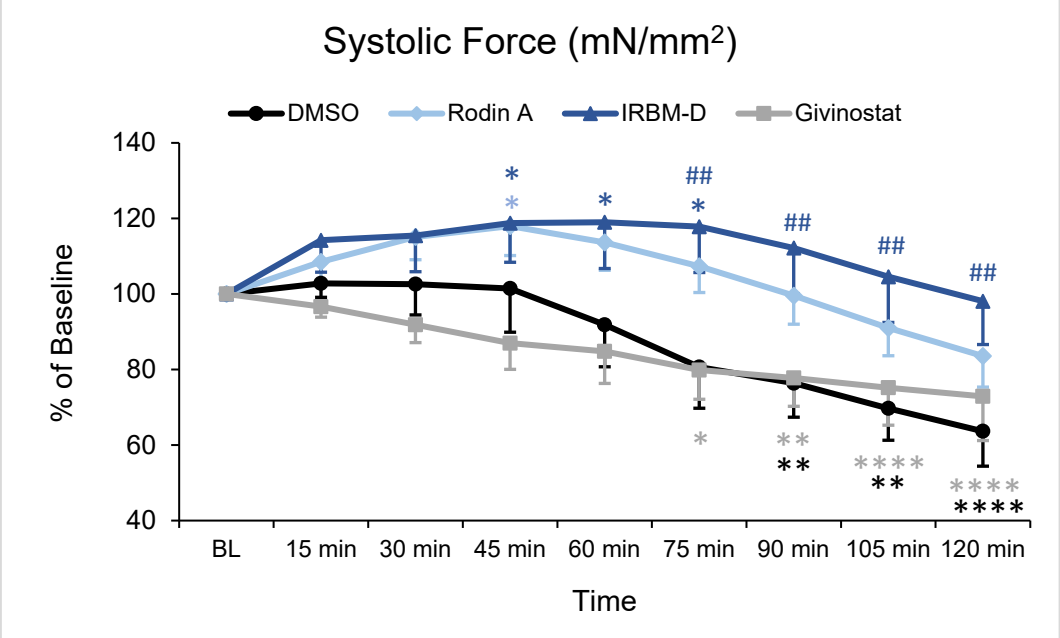

Fig. 8 Investigation of the impact of isoform-selective HDACi on the systolic force in human atrial tissue. The effects of two different selective HDAC inhibitors (blue) and a pan-HDAC inhibitor (grey)

*compared to the control group (black). Both isoform-selective HDAC inhibitors show an acute increase in systolic force. A two-way ANOVA was used for the analysis. * p < 0.05, ** p < 0.01, *** p < 0.001, **** p < 0.0001 individual group vs. their BL, # p < 0.05, ## p < 0.01, ### p < 0.001, #### p < 0.0001 HDAC inhibitor groups vs. control group. Data are means ± SEM.*

In Figure 8 it can be seen that the use of 10µM Rodin A led to a significant increase in systolic force to a maximum value of 118% ± 7.8 of the BL ($p < 0.05$) after 45 minutes. After 60 minutes, the use of IRBM-D caused a maximum increase of up to 119.8% ± 12.3 of the BL ($p < 0.05$). After 120 minutes, the use of IRBM-D led to a score of 98.1% ± 11.5. Both agents already effectuate a positive impact in the first 15 minutes. After reaching the maximum values, the force was sunk continuously with increasing time. The trabeculae incubated with the pan-HDACi Givinostat exhibited a significant decline in systolic force. After 120 minutes, the use of Givinostat caused a value of 72.9% ± 11.7 of the BL ($p < 0.0001$). The systolic force in the control group with DMSO showed almost constant data of about 100% up to 45 minutes, followed by a continuous reduction to 63% ± 9.2 of the BL ($p < 0.0001$). after 120 minutes of incubation. The trabeculae incubated with IRBM-D revealed a significant increase compared to the control group after 75 to 120 minutes ($p < 0.01$).

Similar data were measured with regards to developed force, see Figure 9. The developed force delineates the generated tension during contraction.

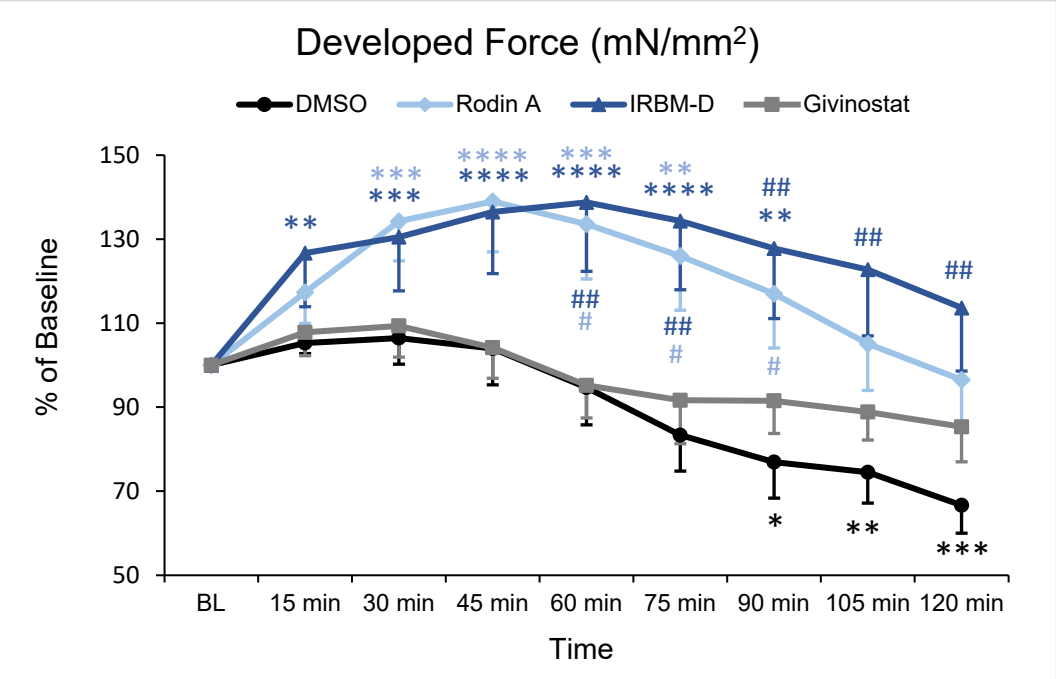

*Fig. 9 Effects of selective HDAC inhibition on atrial muscle trabeculae. The muscle strips incubated with the selective HDAC inhibitors (light blue and dark blue) showed an acute increase in developed force. Instead, trabeculae treated with a pan-HDAC inhibitor (grey) showed no improvement. A two-way ANOWA was used for the analysis. * p < 0.05, ** p < 0.01, *** p < 0.001, **** p < 0.0001 individual group vs. their BL, # p < 0.05, ## p < 0.01, ### p < 0.001, #### p < 0.0001 HDAC inhibitor groups vs. control group. Data are means ± SEM.*

The use of 10 µM Rodin A showed a significant increase in developed force up to a maximum value of 137.6% ±12 of the BL ($p < 0.0001$) after 45 minutes. Moreover, IRBM-D provoked a significant rise of developed force up to 138.8% ± 16.4 of the BL ($p < 0.0001$) after 60 minutes. Meanwhile, the control group and the trabeculae incubated with Givinostat generated no increase at all. Indeed, the control group showed a significant decrease to 66.3% ± 6.6 of the BL ($p < 0.001$) in developed force with time. Compared to the control group, the IRBM-D group indicated a significant improvement after 60 minutes up to 120 minutes ($p < 0.01$). Likewise, the Rodin A treated group showed a significant improvement in developed force compared to the control group between 60 and 90 minutes ($p < 0.05$) of incubation time.

The use of Rodin A, as well as IRBM-D, led to a significant improvement of the kinetic of cardiac muscle contraction represented in dp/dt_{max}, see Figure 10. For the use of Rodin A a maximum value of 138.1% ± 8.8 of the BL ($p < 0.0001$) after 45 minutes was reached. Subsequently, dp/dt_{max} continuously declined till it reached the initial value (100%) after 120 minutes. IRBM-D usage led to a significant rise with a maximum score of 139.8% ± 18.1 relating to the BL value ($p < 0.0001$) after 60 minutes. In contrast, the pan-HDACi Givinostat and the control group with DMSO reached a small, not significant, gain of about 10% within 30 minutes. Subsequently, Givinostat downgrades the kinetic of the trabeculae's contraction to 90% ± 7.1 of the primary value after 120 minutes. In the control group, a significant decrease is reached of about 70% ± 6.7 ($p < 0.001$) after two hours, while the use of specific HDACi groups led to values being obtained of over 100%. The IRMB-D group as well as the Rodin A group demonstrated a significant improvement of dp/dt_{max} compared to the control group (IRBM-D from 75 to 120 minutes $p < 0.01$; Rodin A after 60 and 75 minutes $p < 0.05$).

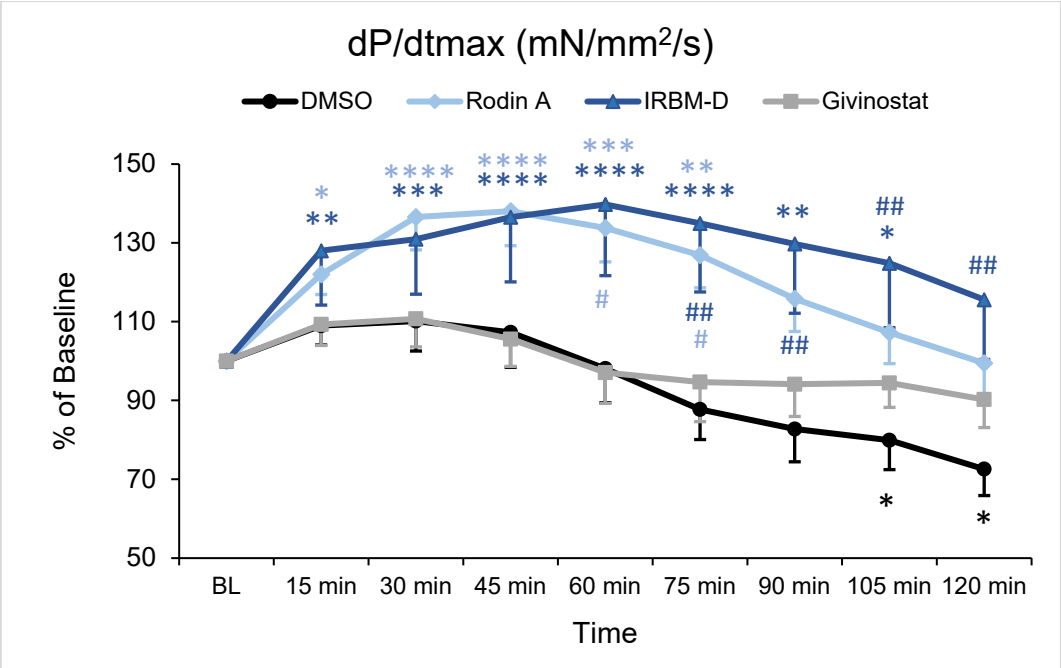

*Fig. 10 The influence of selective HDACi on the myofibril contraction represented in dp/dt$_{max}$. Trabeculae treated with Rodin A and IRBM-D (light and dark blue) exhibit a decisive improvement of about 40% in myofibril contractility compared to the pan-HDAC inhibitor and control group (grey and black). A two-way ANOWA was used for the analysis. * p < 0.05, ** p < 0.01, *** p < 0.001, **** p < 0.0001 individual group vs. their BL, # p < 0.05, ## p < 0.01, ### p < 0.001, #### p < 0.0001 HDAC inhibitor groups vs. control group. Data are means ± SEM.*

From the measured data shown in the figures above, it can be seen that the specific HDACi indicate a significant positive effect on the myocytes' inotropy (systolic force, developed force, dp/dt$_{max}$) within the first 60 minutes.

4.4 Functional effects on diastolic function

The same procedure, as used for the measurement of the contraction parameters mentioned above, was used to record cardiac relaxation parameters. The following parameters were utilized for the measurement: diastolic tension, dp/dt$_{min}$, RT50% Fall, and Tau.

Diastolic force measurement relates to the muscle trabeculae open-circuit voltage. Therefore, the trabeculae were mounted on small hooks. The trabeculae were not placed under tension. The diastolic force was reset to 0 Nm/mm^2 before the stretching steps (zero adjustment). After achieving L$_{max}$, the baseline was defined. The diastolic pressure was examined in relation to the baseline (100%).

All measurements of diastolic tension revealed a clearly visible physiological rundown in the control group, see Figure 11. The rundown effect denominates the loss of power from an in vitro performing muscle trabeculae. This impact is also apparent in the other collected data. Muscle strips incubated with Givinostat and Rodin A exhibited an initial distinct decline of the diastolic tension within the first 40 minutes. Moreover, those incubated with Givinostat showed a significant degression compared to the BL to 48.5% ± 17.1 ($p < 0.001$). Trials with the HDAC inhibitor IRBM-D led to approximately constant values with a significant drop of the diastolic tension compared to the BL after 105 and 120 minutes (105 minutes: 64.4% ± 7.9, $p < 0.05$; 120 minutes: 63.9 ± 9.4, $p < 0.05$).

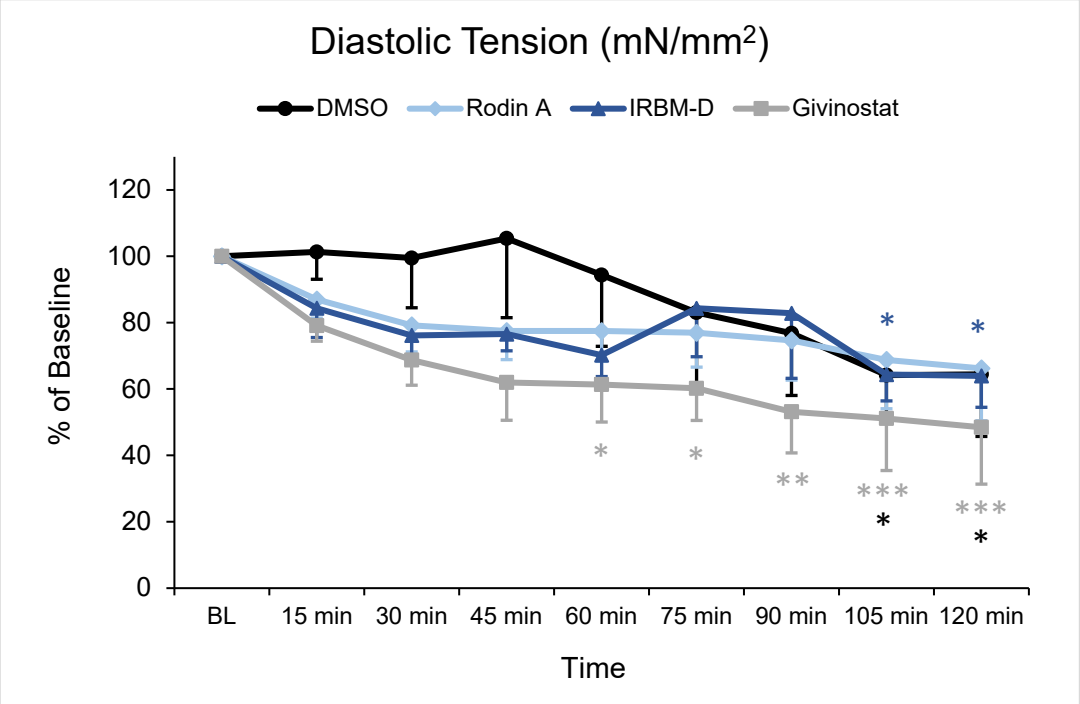

*Fig. 11 Analysis of the influence of isoform-selective HDAC inhibitors on the diastolic tension. The use of the pan-HDAC inhibitor Givinostat (grey) and Rodin A (light blue) caused an initial distinct improvement in diastolic force. The application of HDAC inhibitors IRBM-D (dark blue) led to constant values of diastolic tension. A two-way ANOWA was used for the analysis. * p < 0.05, ** p < 0.01, *** p < 0.001, **** p < 0.0001 individual group vs. their BL, # p < 0.05, ## p < 0.01, ### p < 0.001, #### p < 0.0001 HDAC inhibitor groups vs. control group. Data are means ± SEM.*

A further investigated relaxation parameter was dp/dt_{min}, see Figure 12 for the results. dp/dt_{min} is the maximum value of LV pressure decrease relative to the initial BL value. (85) The raw data are expressed as negative numeric values. So, a percentage increase represents a more negative value.

The use of Rodin A and IRBM-D caused a significant percentage rise of dp/dt_{min} during the whole incubation period (120 min) despite the rundown phenomenon.

IRBM-D led to a maximum increase of dp/dt_{min} to 145.4% ± 18.9 of the BL ($p < 0.0001$) after 45 minutes. Rodin A caused a significant rise of dp/dt_{min} to 150.4% ± 18.2 of the BL ($p < 0.0001$) after 45 minutes. The use of Givinostat led to no significant impact on dp/dt_{min}. The control group led to a significant impairment of dp/dt_{min} with a maximum value of 62.8% ± 6.2 to the BL ($p < 0.001$) after 120 minutes. Compared to the control group, the use of Rodin A as well as IRMB-D caused a significant improvement from 60 minutes to 120 minutes ($p < 0.05$).

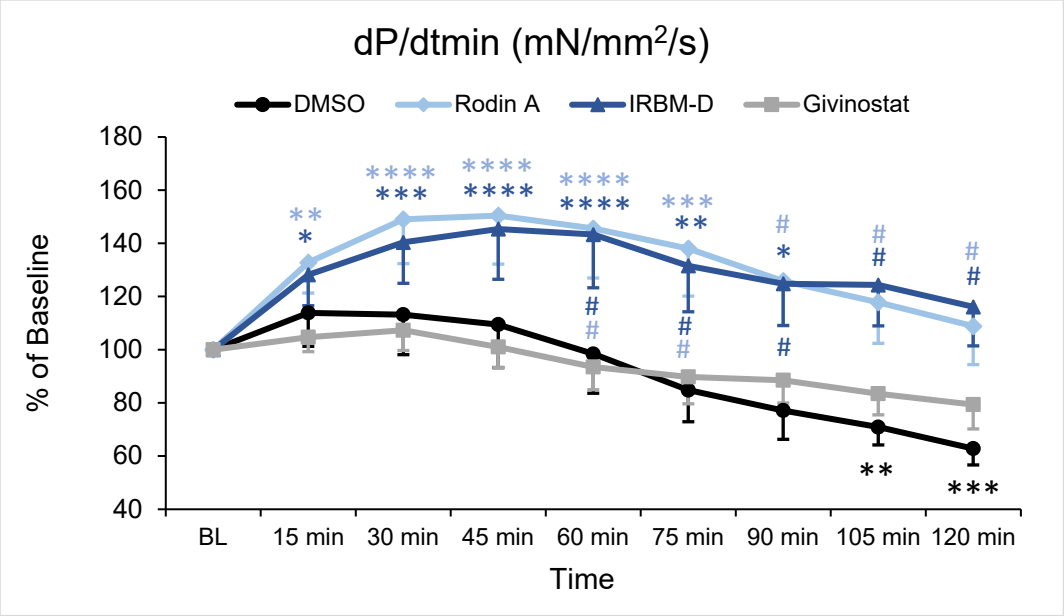

*Fig. 12 Analysis of the impact of the treatment with HDAC inhibitors on myofibril relaxation parameter represented in dp/dt_{min}. Significantly Rodin A (light blue) greatly improves by up to150% the myofibril relaxation. Moreover, IRBM-D (dark blue) shows similar results with an apparent increase in dp/dt_{min}. A two-way ANOWA was used for the analysis. * $p < 0.05$, ** $p < 0.01$, *** $p < 0.001$, **** $p < 0.0001$ individual group vs. their BL, # $p < 0.05$, ## $p < 0.01$, ### $p < 0.001$, #### $p < 0.0001$ HDAC inhibitor groups vs. control group. Data are means ± SEM.*

RT50% Fall is an additional relaxation parameter, see Figure 13 for the results of this part of the study. RT50% Fall describes the time from the peak of contraction to 50% relaxation. (86) The trials with Rodin A showed a shortening with a minimum score of 76% ± 5.2 of the time parameter after the first 15 minutes. The use of IRBM-D caused consistent data of around 100%. Moreover, the use of Givinostat led to values of approximately 100% in the first 60 minutes. Afterwards, the time to 50% relaxation increased. The use of DMSO demonstrated an elongation of time after 45 minutes. Overall, none of these four groups showed any significant values.

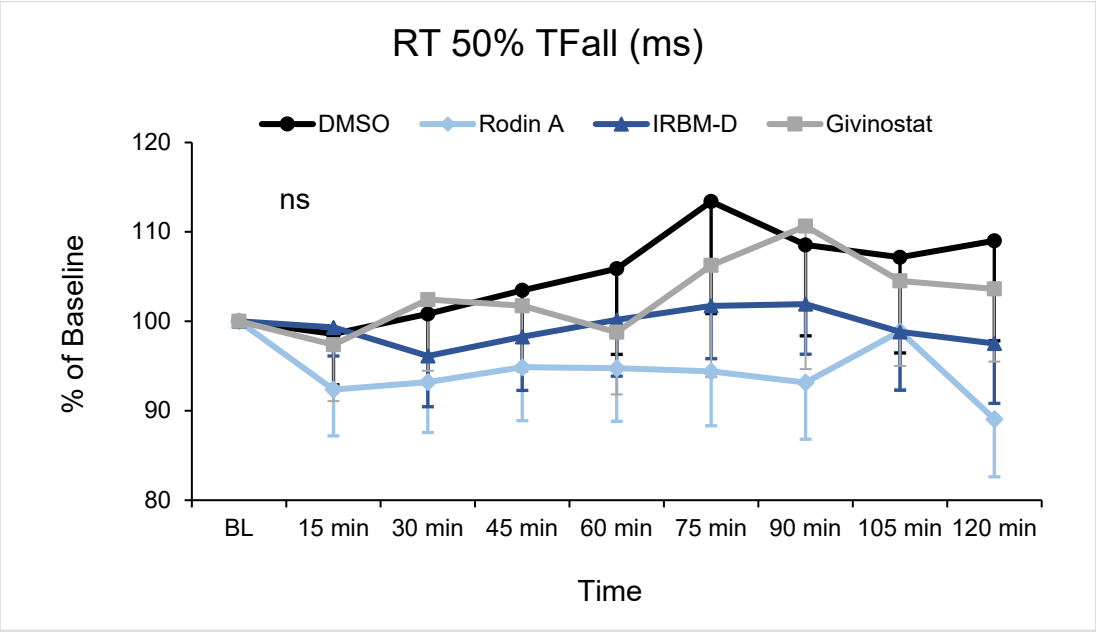

Fig. 13 Effects of selective HDAC inhibitors on the RT 50% TFall parameter. Only the use of Rodin A (light blue) led to a small observable effect in this analysis. The other groups did not show any positive influence. A two-way ANOWA was used for the analysis. ns: not significant. Data are means ± SEM.

The fourth measured relaxation parameter is Tau, see Figure 14. Tau is the time constant of LV isovolumic pressure decrease. (85) The use of Rodin A led to a significant reduction of this parameter. It also caused a significant decrease of Tau to a minimum score of 83.5% ± 9.3 of the BL ($p < 0.01$). There, was also a nearly constant trend of Tau over time with a slight increase for the longest measured times. IRBM-D and Givinostat did cause any significant alterations. The control group demonstrated a continuous incremental increase of Tau during the entire period with a significant increase of Tau to 126.6% ± 11.4 compared to the initial BL value ($p < 0.001$) after 120 minutes. Compared to the control group, the Rodin A group showed a significant improvement of Tau after 120 minutes (90.2% ± 8.1, $p < 0.0001$).

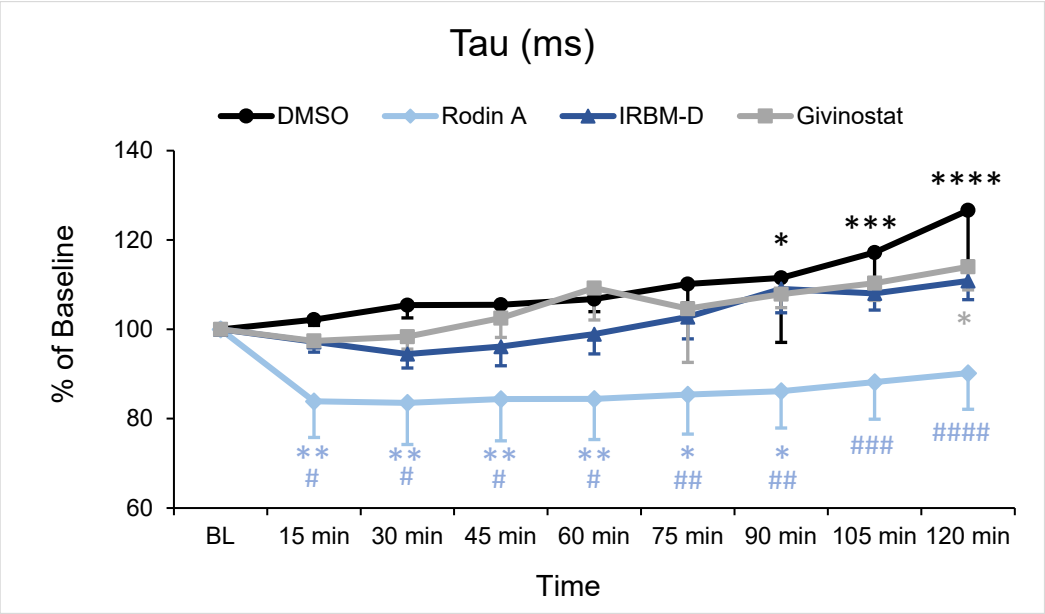

*Fig. 14 The influence of selective HDAC inhibitors on time constant TAU of LV isovolumic pressure decrease. Only the use of the selective HDAC inhibitor Rodin A (light blue) showed an apparent effect on TAU compared to the other intervention groups. A two-way ANOWA was used for the analysis. * p < 0.05, ** p < 0.01, *** p < 0.001, **** p < 0.0001 individual group vs. their BL, # p < 0.05, ## p < 0.01, ### p < 0.001, #### p < 0.0001 HDAC inhibitor groups vs. control group. Data are means ± SEM.*

The specific HDAC inhibitors Rodin A and IRBM-D improved cardiac relaxation parameters as seen from the measured effects. Therefore, both substances had positive influences on myocardial lusitropy.

5. DISCUSSION

This research was focused on the investigation of the effects of two different isoform-selective HDAC inhibitors on human atrial myocardium.

The influence of two specific Class I HDACi and one pan-HDACi on human atrial tissue was analyzed for the first time. IRBM-B inhibits HDAC 1, 2 and 3, while Rodin A inhibits HDAC 1 and 2. The acquired data showed positive effects of selective HDAC inhibition on cardiac contraction and relaxation in multicellular human atrial preparations (trabeculae). The use of IRBM-D and Rodin A revealed a significant increase in systolic force, developed force, and dp/dt_{max} indicative of improved inotropy. Similar findings were obtained from the measurement of the effects of diastolic tension, dp/dt_{min}, and Tau, which are representative for the relaxation parameter. The results exhibited that IRBM-D and Rodin A reduced diastolic tension and enhanced dp/dt_{min}. Indeed, the use of Rodin A significantly improved dp/dt_{min} and there was a reduction of the time constant of LV isovolumic pressure decrease (Tau). Thus, the selective HDACi also improves the lusitropy of the trabeculae.

5.1 HDACi improves diastolic function by improving myofibril relaxation

In several animal studies a positive influence of HDACi on diastolic function have been revealed. Jeong et al. in 2018 demonstrated an enhancement of myofibril relaxation in rodent models with diastolic dysfunction after treatment with the HDAC inhibitor Givinostat. From their measurements it was suggested that Givinostat normalizes LVEDP and directly influences the LV to enhance relaxation. Jeong et al. hypothesized that *" HDAC-dependent alteration in intrinsic relaxation properties of cardiomyocytes contributes to diastolic dysfunction in DSS rats." In their work* LV myofibrils were attached to a force transducer for the investigation, and relaxation kinetics were measured. The results show that HDACi normalizes the linear relaxation phase compared to untreated animals. The linear relaxation phase represents the isovolumic relaxation. In this phase, the filaments' cross-bridging becomes dispensed through the inactivation of filament regulatory proteins. It has been shown that the influence on relaxation is not associated with changes in myofibril calcium sensitivity or titin isoform changing, which controls the

resting tension of myofibrils. The findings were also found to not correspond with alterations in β-MyHC expression. Thus, Jeong et al. suggested that the Givinostat-mediated improvement of relaxation in DSS rats could depend on the direct impact of HDACi on protein function in myocytes without any alteration of protein composition. On the basis of this assumption, HDAC 2 was extracted from the rats. The influence of HDAC 2 deacetylation and acetylation on relaxation duration was analyzed. The results show that myofibrillar protein acetylation influences relaxation. The authors suggested that the decrement of relaxation kinetics by HDACs is an undetected process for the evolution of diastolic dysfunction. (37)

Wallner et al. obtained similar findings on the influence of cardiac kinetic mechanics in a feline model. Thereby, the animals were treated with the HDACi SAHA. Hemodynamic assessment revealed an enhanced inotropic reserve, a smaller ratio between the diastolic period and LV isovolumetric time constant, and a significant reduction in LVEDP. These findings suggest that pan HDAC inhibition improves systolic and diastolic function in these animal models. In addition, it was also reported that SAHA treatment also affects mitochondrial function. (1) Consistent with these findings in the current work the positive effects were revealed of selective HDACi on myofibril contraction and relaxation parameters in human atrial tissue. The isoform-selective HDAC inhibitors IRBM-B and Rodin A inhibit HDAC 1, 2 and 3, and HDAC 1, 2, respectively.

5.2 Posttranslational Modification of non-histone proteins may influence kinetic parameters

HADC inhibitors influence gene expression by posttranslational modification of core histone proteins. The core histone modification regulates the transcriptional response. Transcription alteration can increase collagen synthesis, fibroblast proliferation, and cell cycle protein synthesis, resulting in cardiac fibrosis. (87) The exact pathophysiological process of cardiac remodeling, cardiac fibrosis, and antifibrotic effects remain not entirely understood. (88) Studies in which cardiac fibrosis, anti-remodeling effects, and the efficacy of cardiac mitochondrial gene therapies have been analysed last several weeks to months until appreciable impacts are achieved. (89, 90) Until substantial effects are visible, the duration indicates that HDAC inhibition induced transcriptional response resulting in

antifibrotic effects and diastolic improvement is a long process. Therefore, as represented above in the animal studies, the HDACi-induced posttranslational protein modification partly provokes improvements in myofibril kinetic parameters in atrial muscle strips. Moreover, the experiments on the effects of isoform-selective HDACi on human atrial muscle strips revealed an intensive improvement in systolic and diastolic force, developed force, as well as parameters in myofibril contractility and relaxation. The effects started to occur after the first 15 minutes. Thus, the observed influences have to be based on an acute process in myofibril kinetics. As mentioned before, diastolic improvement through anti-remodeling effects is presumably a procedure lasting up to several weeks. Therefore, the observed acute effect must be based on more than the altered gene expression by posttranslational modification of histone proteins. Indeed, posttranslational modifications of non-histone proteins may explain the acute effects of myofibril relaxation and contractility.

5.3 Ca^{2+} dependent mechanism as the potential contact point

Assuming that the observed effects on myofibril contractility and relaxation are based on acute alterations, other intracellular contact points may influence myofibril kinetics. As mentioned above, Ca^{2+} is involved in a fundamental role in the process of myocyte contractility via ECC. It can be assumed that alterations in this cycle lead to pathophysiological processes in myofibril rhythmic contractility. In particular, SERCA and RyR complexes are essential components in the sequence of ECC. The study of Zima A.V. et al. about Ca^{2+} handling during ECC in heart failure from 2017 involved the assumption that dysfunctions of RyR and SERCA are based on abnormal Ca^{2+} homeostasis in diseased cardiac tissue, such as in heart failure. In this study, the researchers assert that an impaired capability of the SR to store Ca^{2+} can be responsible for restricted contractility in failing hearts. This limited ability of the SR underlies alterations in the expression of various Ca^{2+} transporters and their activity, including SERCA and RyR. (91) Several studies of HF myocytes in the last few years have shown there to be a decline of Ca^{2+} transient amplitude concomitant with reduced Ca^{2+} content in the SR. (92-94) Due to this finding, Zima A.V. et al. have supposed that one of the leading causes of reduced SR Ca^{2+} discharge and declined contraction in HF is a disturbed uptake of

Ca^{2+} in the SR. (91) This suggests that impairment of SERCA leads to restricted Ca^{2+} uptake in the SR and to degraded energy production for myofilaments. Thus, contraction and relaxation of the myofilaments can be disturbed. On the basis of the assumption that HDAC inhibitors also affect non-histone proteins and the observed improvement in myofibril kinetics, HDACi may impact SERCA's activity level, affecting the Ca^{2+} homeostasis and ATP and availability for movement of the myofilaments. For example, in the study from Meraviglia et al. it was shown that there is a relation between HDACs and the activity and function of SERCA2 by using SAHA. (95) In addition, on the basis of the results of other studies a connection has been demonstrated between the activity of SERCA2 and the inhibition of deacetylation of different lysine residues. (96, 97) Moreover, in studies on the treatment of different cancer cell lines it has been detected that HDAC inhibitors increases histone H3 acetylation at the promoter of ATP2A3 gene encoding the enzyme SERCA3. The increased acetylation led to a rise of SERCA3 mRNA expression. However, the exact underlying molecular process of SERCA3 mRNA upregulation is not clear. (98) HDACi may also influence the function or activity level of other Ca^{2+} transporters like RyR or NCX, leading to calcium concentration and homeostasis alterations. In recent studies it has been demonstrated that there is a relation between increased expression of class II HDACs .and RyR1. (99, 100) However, there are no published articles about the effects of HDAC inhibitors of RyR in cardiac myocytes.

5.4 Potential impact of HDACi on myofilaments

The intracellular homeostasis of Ca^{2+} and ATP supply are fundamental components of the mobility of the myofilaments, known as electromechanical coupling. As mentioned above, the Ca^{2+} release during the action potential correlates with the interaction between myosin and actin filaments triggering the contraction of the myocyte. This process suggests that alterations of the Ca^{2+} availability for the electromechanical coupling and changes in the calcium sensitivity can lead to modified bindings between actin and myosin. The main focus has been on myosin II's function, representing the heart muscles' molecular motor. Myosin regulatory light chains (RLC) and myosin essential light chains (ELC) belong to the EF-hands Ca^{2+} -binding proteins, but myosin ELC has lost the

ability to bind. Consequently, altered intracellular Ca^{2+}-homeostasis primarily affects the myosin RLC, a regulator subunit of cardiac muscle myosin. (101) Thereby, the myofilament function and myofilament stiffness based on the actin-myosin complex can be altered and may be improved through increased calcium sensitivity. In addition to the potential influence of the substrates on myofibril contractility via calcium sensitivity, it is described above that HDAC inhibitors can influence proteins via acetylation. Moreover, it is possible that HDAC inhibitors also exert influence on parts of the myofilaments by inhibiting deacetylation and regulating myocytes and cardiac function.

5.5 The clinical use

Currently, only non-specific HDAC inhibitors are commercially available and approved as anti-cancer drugs for multiple myeloma and T-cell lymphomas. Non-specific means that a broad variety of HDAC classes are inhibited. Thus, these agents are also associated with class-related adverse effects. This includes myelosuppression, diarrhoea, nausea, fatigue, and abnormalities in the electrocardiogram, like ST-T irregularities and QTc interval prolongation. (102) In different studies (21, 103-105) it has been suggested that predominantly class I, HDAC 1, 2, and 3, are responsible for cardiac remodeling, hypertrophy, and cardiac failure. For example, it was also demonstrated that inhibition of class I HDACs suppresses cardiac hypertrophy. The underlying process is still undefined but might be based on a de-depression of antihypertrophic genes. (89, 105)

5.6 Limitations and Strengths

HFpEF is a complex, heterogeneous clinical syndrome with typical symptoms like fatigue, dyspnea, and peripheral edema. It is impossible to mimic all critical features of HFpEF in model systems. In the work for this thesis, only right atrial tissue derived from patients with normal ejection fraction was utilized. Thus, tissue alterations due to enlargement of the LA or increased LVEDP were not considered. The availability of human heart tissue is a limiting factor and it partly depended on the surgical procedure and the method of connecting the heart to the heart-lung-machine in this study. However, the actual use of human heart tissue –

even if this is “just” right atrial tissue - is a strength of this study. The trabeculae bathed in the puffer solution were electrically stimulated at 1 Hz. Thereby, an in-vitro model with physiological conditions was formed. Nevertheless, studies with human left ventricular tissue would be more meaningful.
In the work for this thesis, it has been shown that isoform-selective HDAC inhibitors positively impact the twitch kinetics of cardiac muscle strips. HDAC inhibitors effectuated a clear improvement of contractility as well as relaxation parameters. Nevertheless, these results should be critically considered because only functional parameters were measured. Thus, various questions about the molecular influence of isoform-selective HDAC inhibitors on human cardiac tissue still need to be clarified.

Further insights into the biomolecular impact of HDAC inhibitors on myocytes can be found in the 2022 article *“HDAC Inhibition Regulates Cardiac Function by Increasing Myofilament Calcium Sensitivity and Decreasing Diastolic Tension”* written by Eaton et al.. (106) Although the authors reported there to be a direct control of HDAC inhibition on cardiac contractility and improved myofibril relaxation, some questions remained unanswered such as the underlying mechanism leading to the improved passive tension. Some intracellular proceedings are also still unclear. The observed functional improvements might be based on changes in the structural protein titin or alterations of the microtubules as part of the cytoskeleton. However, there have been no experiments undertaken on the effects of isoform-selective HDAC inhibitors on titin or microtubules. Therefore, further studies are warranted for targeted research of the molecular changes.

5.7 Future outlook

Since the compounds have been tested exclusively in atrial human myocardium, no conclusions can be drawn about the effects on ventricular myocardium. Further studies are needed for an investigation of the systemic and ventricular effects of selective HDACi. In addition, it has to be tested if the tolerability of isoform-selective HDAC inhibitors is better than the tolerability of pan-HDAC inhibitors and which side effects are induced by isoform-selective HDAC inhibitors.

6. CONCLUSION

Two-different isoform HDAC inhibitors and a pan-HDAC inhibitor were tested on human myocardium for the first time. On the basis of an approach using live twitching human atrial trabeculae, it was revealed in this work that there is an improvement in myofibril contractility and relaxation. In particular, the non-commercial available isoform-selective HDAC inhibitors exhibited significant enhancements of diverse systolic and diastolic parameters. In previous studies involving pan-HDAC inhibitors adverse effects were demonstrated such as myelosuppression, QT-prolongation, and gastrointestinal symptoms. A more isoform-specific approach may be required to increase the safety profile. Therefore, the two isoform-selective HDAC inhibitors were developed and tested in this work. An isoform-selective effectiveness of substrates is a promising approach for the development of new therapeutic agents for treating heart failure, especially HFpEF. These findings suggest that isoform-selective HDAC inhibitors are promising for treating heart failure patients.

7. BIBLIOGRAPHY

1. Wallner M, Eaton DM, Berretta RM, Liesinger L, Schittmayer M, Gindlhuber J, et al. HDAC inhibition improves cardiopulmonary function in a feline model of diastolic dysfunction. Sci Transl Med. 2020;12(525).

2. Tammen SA, Friso S, Choi SW. Epigenetics: the link between nature and nurture. Mol Aspects Med. 2013;34(4):753-64.

3. Jaenisch R, Bird A. Epigenetic regulation of gene expression: how the genome integrates intrinsic and environmental signals. Nat Genet. 2003;33 Suppl:245-54.

4. Kouzarides T. Chromatin modifications and their function. Cell. 2007;128(4):693-705.

5. Luger K, Mader AW, Richmond RK, Sargent DF, Richmond TJ. Crystal structure of the nucleosome core particle at 2.8 A resolution. Nature. 1997;389(6648):251-60.

6. Zhao Y, Garcia BA. Comprehensive Catalog of Currently Documented Histone Modifications. Cold Spring Harb Perspect Biol. 2015;7(9):a025064.

7. Wang Y, Miao X, Liu Y, Li F, Liu Q, Sun J, et al. Dysregulation of histone acetyltransferases and deacetylases in cardiovascular diseases. Oxid Med Cell Longev. 2014;2014:641979.

8. Berezin A. Epigenetics in heart failure phenotypes. BBA Clin. 2016;6:31-7.

9. Yang XJ, Seto E. HATs and HDACs: from structure, function and regulation to novel strategies for therapy and prevention. Oncogene. 2007;26(37):5310-8.

10. Papait R, Serio S, Condorelli G. Role of the Epigenome in Heart Failure. Physiol Rev. 2020;100(4):1753-77.

11. Chuang DM, Leng Y, Marinova Z, Kim HJ, Chiu CT. Multiple roles of HDAC inhibition in neurodegenerative conditions. Trends Neurosci. 2009;32(11):591-601.

12. Yang XJ, Seto E. Lysine acetylation: codified crosstalk with other posttranslational modifications. Mol Cell. 2008;31(4):449-61.

13. Bonkowski MS, Sinclair DA. Slowing ageing by design: the rise of NAD(+) and sirtuin-activating compounds. Nat Rev Mol Cell Biol. 2016;17(11):679-90.

14. Allfrey VG, Faulkner R, Mirsky AE. Acetylation and Methylation of Histones and Their Possible Role in the Regulation of Rna Synthesis. Proc Natl Acad Sci U S A. 1964;51(5):786-94.

15. Struhl K. Histone acetylation and transcriptional regulatory mechanisms. Genes Dev. 1998;12(5):599-606.

16. Kim SY, Morales CR, Gillette TG, Hill JA. Epigenetic regulation in heart failure. Curr Opin Cardiol. 2016;31(3):255-65.

17. Zhang L, Qin X, Zhao Y, Fast L, Zhuang S, Liu P, et al. Inhibition of histone deacetylases preserves myocardial performance and prevents cardiac remodeling through stimulation of endogenous angiomyogenesis. J Pharmacol Exp Ther. 2012;341(1):285-93.

18. Colussi C, Illi B, Rosati J, Spallotta F, Farsetti A, Grasselli A, et al. Histone deacetylase inhibitors: keeping momentum for neuromuscular and cardiovascular diseases treatment. Pharmacol Res. 2010;62(1):3-10.

19. Dingar D, Konecny F, Zou J, Sun X, von Harsdorf R. Anti-apoptotic function of the E2F transcription factor 4 (E2F4)/p130, a member of retinoblastoma gene family in cardiac myocytes. J Mol Cell Cardiol. 2012;53(6):820-8.

20. Kee HJ, Kook H. Roles and targets of class I and IIa histone deacetylases in cardiac hypertrophy. J Biomed Biotechnol. 2011;2011:928326.

21. Trivedi CM, Luo Y, Yin Z, Zhang M, Zhu W, Wang T, et al. Hdac2 regulates the cardiac hypertrophic response by modulating Gsk3 beta activity. Nat Med. 2007;13(3):324-31.

22. Singh N, Trivedi CM, Lu M, Mullican SE, Lazar MA, Epstein JA. Histone deacetylase 3 regulates smooth muscle differentiation in neural crest cells and development of the cardiac outflow tract. Circ Res. 2011;109(11):1240-9.

23. Kee HJ, Bae EH, Park S, Lee KE, Suh SH, Kim SW, et al. HDAC inhibition suppresses cardiac hypertrophy and fibrosis in DOCA-salt hypertensive rats via regulation of HDAC6/HDAC8 enzyme activity. Kidney Blood Press Res. 2013;37(4-5):229-39.

24. Raghunathan S, Goyal RK, Patel BM. Selective inhibition of HDAC2 by magnesium valproate attenuates cardiac hypertrophy. Can J Physiol Pharmacol. 2017;95(3):260-7.

25. Li P, Ge J, Li H. Lysine acetyltransferases and lysine deacetylases as targets for cardiovascular disease. Nat Rev Cardiol. 2020;17(2):96-115.

26. Shanmugam G, Rakshit S, Sarkar K. HDAC inhibitors: Targets for tumor therapy, immune modulation and lung diseases. Transl Oncol. 2022;16:101312.

27. Fantin VR, Richon VM. Mechanisms of resistance to histone deacetylase inhibitors and their therapeutic implications. Clin Cancer Res. 2007;13(24):7237-42.

28. Duvic M, Vu J. Vorinostat in cutaneous T-cell lymphoma. Drugs Today (Barc). 2007;43(9):585-99.

29. Center for Drugs and Biologics (U.S.), Center for Drug Evaluation and Research (U.S.), Center for Drug Evaluation and Research (U.S.). Office of Management., Center for Drug Evaluation and Research (U.S.). Division of Drug Information Resources., Center for Drug Evaluation and Research (U.S.). Division of Data Management and Services., Center for Drug Evaluation and Research (U.S.). Office of Generic Drugs. Approved drug products with therapeutic equivalence evaluations. Rockville, Md.: U.S. Dept. of Health and Human

Services, Public Health Service, Food and Drug Administration, Center for Drugs and Biologics; 1985. p. volumes.

30. Mody D, Bouckaert J, Savvides SN, Gupta V. Rational Design and Development of HDAC Inhibitors for Breast Cancer Treatment. Curr Pharm Des. 2021;27(45):4610-29.

31. Spartalis E, Kotrotsios K, Chrysikos D, Spartalis M, Paschou SA, Schizas D, et al. Histone Deacetylase Inhibitors and Papillary Thyroid Cancer. Curr Pharm Des. 2021;27(18):2199-208.

32. Dai Y, Wei T, Shen Z, Bei Y, Lin H, Dai H. Classical HDACs in the regulation of neuroinflammation. Neurochem Int. 2021;150:105182.

33. Yang J, Grafton F, Ranjbarvaziri S, Budan A, Farshidfar F, Cho M, et al. Phenotypic screening with deep learning identifies HDAC6 inhibitors as cardioprotective in a BAG3 mouse model of dilated cardiomyopathy. Sci Transl Med. 2022;14(652):eabl5654.

34. Yoon S, Eom GH. HDAC and HDAC Inhibitor: From Cancer to Cardiovascular Diseases. Chonnam Med J. 2016;52(1):1-11.

35. Liu CF, Tang WHW. Epigenetics in Cardiac Hypertrophy and Heart Failure. JACC Basic Transl Sci. 2019;4(8):976-93.

36. McKinsey TA. Therapeutic potential for HDAC inhibitors in the heart. Annu Rev Pharmacol Toxicol. 2012;52:303-19.

37. Jeong MY, Lin YH, Wennersten SA, Demos-Davies KM, Cavasin MA, Mahaffey JH, et al. Histone deacetylase activity governs diastolic dysfunction through a nongenomic mechanism. Sci Transl Med. 2018;10(427).

38. Conceicao G, Heinonen I, Lourenco AP, Duncker DJ, Falcao-Pires I. Animal models of heart failure with preserved ejection fraction. Neth Heart J. 2016;24(4):275-86.

39. Sharifov OF, Schiros CG, Aban I, Denney TS, Gupta H. Diagnostic Accuracy of Tissue Doppler Index E/e' for Evaluating Left Ventricular Filling Pressure and Diastolic Dysfunction/Heart Failure With Preserved Ejection Fraction: A Systematic Review and Meta-Analysis. J Am Heart Assoc. 2016;5(1).

40. McDonagh TA, Metra M, Adamo M, Gardner RS, Baumbach A, Bohm M, et al. 2021 ESC Guidelines for the diagnosis and treatment of acute and chronic heart failure. Eur Heart J. 2021;42(36):3599-726.

41. Anker SD, Butler J, Filippatos G, Ferreira JP, Bocchi E, Bohm M, et al. Empagliflozin in Heart Failure with a Preserved Ejection Fraction. N Engl J Med. 2021;385(16):1451-61.

42. Solomon SD, McMurray JJV, Claggett B, de Boer RA, DeMets D, Hernandez AF, et al. Dapagliflozin in Heart Failure with Mildly Reduced or Preserved Ejection Fraction. N Engl J Med. 2022;387(12):1089-98.

43. Heidenreich PA, Bozkurt B, Aguilar D, Allen LA, Byun JJ, Colvin MM, et al. 2022 AHA/ACC/HFSA Guideline for the Management of Heart Failure: Executive Summary: A Report of the American College of Cardiology/American Heart Association Joint Committee on Clinical Practice Guidelines. Circulation. 2022;145(18):e876-e94.

44. Tsao CW, Lyass A, Enserro D, Larson MG, Ho JE, Kizer JR, et al. Temporal Trends in the Incidence of and Mortality Associated With Heart Failure With Preserved and Reduced Ejection Fraction. JACC Heart Fail. 2018;6(8):678-85.

45. Chan MM, Lam CS. How do patients with heart failure with preserved ejection fraction die? Eur J Heart Fail. 2013;15(6):604-13.

46. Bozkurt B, Coats AJS, Tsutsui H, Abdelhamid CM, Adamopoulos S, Albert N, et al. Universal definition and classification of heart failure: a report of the Heart Failure Society of America, Heart Failure Association of the European Society of Cardiology, Japanese Heart Failure Society and Writing Committee of the Universal Definition of Heart Failure: Endorsed by the Canadian Heart Failure Society, Heart Failure Association of India, Cardiac Society of Australia and New Zealand, and Chinese Heart Failure Association. Eur J Heart Fail. 2021;23(3):352-80.

47. McMurray JJ, Packer M, Desai AS, Gong J, Lefkowitz MP, Rizkala AR, et al. Angiotensin-neprilysin inhibition versus enalapril in heart failure. N Engl J Med. 2014;371(11):993-1004.

48. Zannad F, McMurray JJ, Krum H, van Veldhuisen DJ, Swedberg K, Shi H, et al. Eplerenone in patients with systolic heart failure and mild symptoms. N Engl J Med. 2011;364(1):11-21.

49. Packer M, Poole-Wilson PA, Armstrong PW, Cleland JG, Horowitz JD, Massie BM, et al. Comparative effects of low and high doses of the angiotensin-converting enzyme inhibitor, lisinopril, on morbidity and mortality in chronic heart failure. ATLAS Study Group. Circulation. 1999;100(23):2312-8.

50. Bristow MR, Gilbert EM, Abraham WT, Adams KF, Fowler MB, Hershberger RE, et al. Carvedilol produces dose-related improvements in left ventricular function and survival in subjects with chronic heart failure. MOCHA Investigators. Circulation. 1996;94(11):2807-16.

51. McMurray JJV, Solomon SD, Inzucchi SE, Kober L, Kosiborod MN, Martinez FA, et al. Dapagliflozin in Patients with Heart Failure and Reduced Ejection Fraction. N Engl J Med. 2019;381(21):1995-2008.

52. Pitt B, Pfeffer MA, Assmann SF, Boineau R, Anand IS, Claggett B, et al. Spironolactone for heart failure with preserved ejection fraction. N Engl J Med. 2014;370(15):1383-92.

53. Solomon SD, McMurray JJV, Anand IS, Ge J, Lam CSP, Maggioni AP, et al. Angiotensin-Neprilysin Inhibition in Heart Failure with Preserved Ejection Fraction. N Engl J Med. 2019;381(17):1609-20.

54. Lund LH, Claggett B, Liu J, Lam CS, Jhund PS, Rosano GM, et al. Heart failure with mid-range ejection fraction in CHARM: characteristics, outcomes and effect of candesartan across the entire ejection fraction spectrum. Eur J Heart Fail. 2018;20(8):1230-9.

55. Upadhya B, Kitzman DW. Heart failure with preserved ejection fraction: New approaches to diagnosis and management. Clin Cardiol. 2020;43(2):145-55.

56. Gerber Y, Weston SA, Redfield MM, Chamberlain AM, Manemann SM, Jiang R, et al. A contemporary appraisal of the heart failure epidemic in Olmsted County, Minnesota, 2000 to 2010. JAMA Intern Med. 2015;175(6):996-1004.

57. Dunlay SM, Roger VL, Redfield MM. Epidemiology of heart failure with preserved ejection fraction. Nat Rev Cardiol. 2017;14(10):591-602.

58. Borlaug BA. Evaluation and management of heart failure with preserved ejection fraction. Nat Rev Cardiol. 2020;17(9):559-73.

59. Reddy YNV, Melenovsky V, Redfield MM, Nishimura RA, Borlaug BA. High-Output Heart Failure: A 15-Year Experience. J Am Coll Cardiol. 2016;68(5):473-82.

60. Nair N. Epidemiology and pathogenesis of heart failure with preserved ejection fraction. Rev Cardiovasc Med. 2020;21(4):531-40.

61. Borlaug BA. The pathophysiology of heart failure with preserved ejection fraction. Nat Rev Cardiol. 2014;11(9):507-15.

62. Ma C, Luo H, Fan L, Liu X, Gao C. Heart failure with preserved ejection fraction: an update on pathophysiology, diagnosis, treatment, and prognosis. Braz J Med Biol Res. 2020;53(7):e9646.

63. Borlaug BA, Nishimura RA, Sorajja P, Lam CS, Redfield MM. Exercise hemodynamics enhance diagnosis of early heart failure with preserved ejection fraction. Circ Heart Fail. 2010;3(5):588-95.

64. Pieske B, Tschope C, de Boer RA, Fraser AG, Anker SD, Donal E, et al. How to diagnose heart failure with preserved ejection fraction: the HFA-PEFF diagnostic algorithm: a consensus recommendation from the Heart Failure Association (HFA) of the European Society of Cardiology (ESC). Eur Heart J. 2019;40(40):3297-317.

65. Reddy YNV, Carter RE, Obokata M, Redfield MM, Borlaug BA. A Simple, Evidence-Based Approach to Help Guide Diagnosis of Heart Failure With Preserved Ejection Fraction. Circulation. 2018;138(9):861-70.

66. Zirkl J. Herzinsuffizienz (HI) schwerwiegende Erkrankung im Vormarsch 2021 [Available from: https://www.herzverband-stmk.at/herzinsuffizienz-hl-schwerwiegende-erkrankung-im-vormarsch/.

67. Emmons-Bell S, Johnson C, Roth G. Prevalence, incidence and survival of heart failure: a systematic review. Heart. 2022;108(17):1351-60.

68. Groenewegen A, Rutten FH, Mosterd A, Hoes AW. Epidemiology of heart failure. Eur J Heart Fail. 2020;22(8):1342-56.

69. Roger VL. Epidemiology of Heart Failure: A Contemporary Perspective. Circ Res. 2021;128(10):1421-34.

70. Omote K, Verbrugge FH, Borlaug BA. Heart Failure with Preserved Ejection Fraction: Mechanisms and Treatment Strategies. Annu Rev Med. 2022;73:321-37.

71. Lesyuk W, Kriza C, Kolominsky-Rabas P. Cost-of-illness studies in heart failure: a systematic review 2004-2016. BMC Cardiovasc Disord. 2018;18(1):74.

72. Iliesiu AM, Hodorogea AS. Treatment of Heart Failure with Preserved Ejection Fraction. Adv Exp Med Biol. 2018;1067:67-87.

73. Passantino A, Rizzo C, Scrutinio D, Palazzuoli A. Diabetes and SGLT2-iss inhibitors in patients with heart failure with preserved or mid-range left ventricular ejection fractions. Heart Fail Rev. 2021.

74. Nerbonne JM, Kass RS. Molecular physiology of cardiac repolarization. Physiol Rev. 2005;85(4):1205-53.

75. Hennis K, Biel M, Wahl-Schott C, Fenske S. Beyond pacemaking: HCN channels in sinoatrial node function. Prog Biophys Mol Biol. 2021;166:51-60.

76. Fearnley CJ, Roderick HL, Bootman MD. Calcium signaling in cardiac myocytes. Cold Spring Harb Perspect Biol. 2011;3(11):a004242.

77. Pfeiffer ER, Tangney JR, Omens JH, McCulloch AD. Biomechanics of cardiac electromechanical coupling and mechanoelectric feedback. J Biomech Eng. 2014;136(2):021007.

78. Blatter LA, Kanaporis G, Martinez-Hernandez E, Oropeza-Almazan Y, Banach K. Excitation-contraction coupling and calcium release in atrial muscle. Pflugers Arch. 2021;473(3):317-29.

79. Maack C, O'Rourke B. Excitation-contraction coupling and mitochondrial energetics. Basic Res Cardiol. 2007;102(5):369-92.

80. Lamb GD. Excitation-contraction coupling in skeletal muscle: comparisons with cardiac muscle. Clin Exp Pharmacol Physiol. 2000;27(3):216-24.

81. Gordon AM, Homsher E, Regnier M. Regulation of contraction in striated muscle. Physiol Rev. 2000;80(2):853-924.

82. Solaro RJ, Rarick HM. Troponin and tropomyosin: proteins that switch on and tune in the activity of cardiac myofilaments. Circ Res. 1998;83(5):471-80.

83. Watanabe Y, Iwamoto T, Matsuoka I, Ohkubo S, Ono T, Watano T, et al. Inhibitory effect of 2,3-butanedione monoxime (BDM) on Na(+)/Ca(2+) exchange current in guinea-pig cardiac ventricular myocytes. Br J Pharmacol. 2001;132(6):1317-25.

84. Delicce AV, Makaryus AN. Physiology, Frank Starling Law. StatPearls. Treasure Island (FL)2023.

85. Henning RJ, Khalil I. Autonomic nervous stimulation affects left ventricular relaxation more than left ventricular contraction. J Auton Nerv Syst. 1989;28(1):15-25.

86. Bertoni AG, Adrian S, Mankad S, Silverman HS. Impaired posthypoxic relaxation in single cardiac myocytes: role of intracellular pH and inorganic phosphate. Cardiovasc Res. 1993;27(11):1983-90.

87. Travers JG, Wennersten SA, Pena B, Bagchi RA, Smith HE, Hirsch RA, et al. HDAC Inhibition Reverses Preexisting Diastolic Dysfunction and Blocks Covert Extracellular Matrix Remodeling. Circulation. 2021;143(19):1874-90.

88. Liu M, Lopez de Juan Abad B, Cheng K. Cardiac fibrosis: Myofibroblast-mediated pathological regulation and drug delivery strategies. Adv Drug Deliv Rev. 2021;173:504-19.

89. Akio Monji YKB, Haruya Kawase, Morihiko Aoyama and Toyoaki Murohara. Abstract 205: Mitochondrial Sirt3 Is Upregulated By Glucagon-like Peptide-1 Receptor Activation And Contributes To Reversal Of Cardiac Mitochondrial Remodeling Induced By Type 2 Diabetes. Circulation Research2018 [Available from: https://www.ahajournals.org/doi/10.1161/res.115.suppl_1.205.

90. Korpela H, Jarvelainen N, Siimes S, Lampela J, Airaksinen J, Valli K, et al. Gene therapy for ischaemic heart disease and heart failure. J Intern Med. 2021;290(3):567-82.

91. Zima AV, Bovo E, Mazurek SR, Rochira JA, Li W, Terentyev D. Ca handling during excitation-contraction coupling in heart failure. Pflugers Arch. 2014;466(6):1129-37.

92. Hobai IA, O'Rourke B. Decreased sarcoplasmic reticulum calcium content is responsible for defective excitation-contraction coupling in canine heart failure. Circulation. 2001;103(11):1577-84.

93. Lindner M, Erdmann E, Beuckelmann DJ. Calcium content of the sarcoplasmic reticulum in isolated ventricular myocytes from patients with terminal heart failure. J Mol Cell Cardiol. 1998;30(4):743-9.

94. Piacentino V, 3rd, Weber CR, Chen X, Weisser-Thomas J, Margulies KB, Bers DM, et al. Cellular basis of abnormal calcium transients of failing human ventricular myocytes. Circ Res. 2003;92(6):651-8.

95. Meraviglia V, Bocchi L, Sacchetto R, Florio MC, Motta BM, Corti C, et al. HDAC Inhibition Improves the Sarcoendoplasmic Reticulum Ca(2+)-ATPase Activity in Cardiac Myocytes. Int J Mol Sci. 2018;19(2).

96. Gorski PA, Jang SP, Jeong D, Lee A, Lee P, Oh JG, et al. Role of SIRT1 in Modulating Acetylation of the Sarco-Endoplasmic Reticulum Ca(2+)-ATPase in Heart Failure. Circ Res. 2019;124(9):e63-e80.

97. Kho C, Lee A, Jeong D, Oh JG, Chaanine AH, Kizana E, et al. SUMO1-dependent modulation of SERCA2a in heart failure. Nature. 2011;477(7366):601-5.

98. Hernandez-Oliveras A, Izquierdo-Torres E, Meneses-Morales I, Rodriguez G, Zarain-Herzberg A, Santiago-Garcia J. Histone deacetylase inhibitors promote ATP2A3 gene expression in hepatocellular carcinoma cells: p300 as a transcriptional regulator. Int J Biochem Cell Biol. 2019;113:8-16.

99. Ruiz A, Benucci S, Duthaler U, Bachmann C, Franchini M, Noreen F, et al. Improvement of muscle strength in a mouse model for congenital myopathy treated with HDAC and DNA methyltransferase inhibitors. Elife. 2022;11.

100. Rokach O, Sekulic-Jablanovic M, Voermans N, Wilmshurst J, Pillay K, Heytens L, et al. Epigenetic changes as a common trigger of muscle weakness in congenital myopathies. Hum Mol Genet. 2015;24(16):4636-47.

101. Sitbon YH, Yadav S, Kazmierczak K, Szczesna-Cordary D. Insights into myosin regulatory and essential light chains: a focus on their roles in cardiac and skeletal muscle function, development and disease. J Muscle Res Cell Motil. 2020;41(4):313-27.

102. Shah RR. Safety and Tolerability of Histone Deacetylase (HDAC) Inhibitors in Oncology. Drug Saf. 2019;42(2):235-45.

103. Kee HJ, Eom GH, Joung H, Shin S, Kim JR, Cho YK, et al. Activation of histone deacetylase 2 by inducible heat shock protein 70 in cardiac hypertrophy. Circ Res. 2008;103(11):1259-69.

104. Montgomery RL, Davis CA, Potthoff MJ, Haberland M, Fielitz J, Qi X, et al. Histone deacetylases 1 and 2 redundantly regulate cardiac morphogenesis, growth, and contractility. Genes Dev. 2007;21(14):1790-802.

105. Gallo P, Latronico MV, Gallo P, Grimaldi S, Borgia F, Todaro M, et al. Inhibition of class I histone deacetylase with an apicidin derivative prevents cardiac hypertrophy and failure. Cardiovasc Res. 2008;80(3):416-24.

106. Eaton DM, Martin TG, Kasa M, Djalinac N, Ljubojevic-Holzer S, Von Lewinski D, et al. HDAC Inhibition Regulates Cardiac Function by Increasing Myofilament Calcium Sensitivity and Decreasing Diastolic Tension. Pharmaceutics. 2022;14(7).

8. APPENDIX

8.1 Measured values with 10µM Rodin A

Diastolic Force	131120 CH7	201120 CH7	271120 CH8	301120 CH5	111220 CH6	160221 CH6	100321 CH6	230321 CH7	Mittelwert	Stabw	SEM
Lmax (%)	100,00	100,00	100,00	100,00	100,00	100,00	100,00	100,00	100,00	0,00	0,00
15min	56,39	76,29	103,70	87,07	101,60	80,74	99,34	90,66	86,97	15,80	5,59
30	36,17	68,37	95,00	83,28	108,74	70,92	98,46	72,51	79,18	22,65	8,01
45	39,85	68,77	84,32	89,17	114,19	60,73	101,54	61,13	77,46	24,35	8,61
60	46,11	59,06	90,01	96,01	115,13	56,80	100,81	55,80	77,46	25,87	9,14
75	39,69	45,60	100,80	87,42	116,92	59,74	104,47	60,88	76,94	29,18	10,31
90	40,95	29,13	102,30	91,16	117,58	54,46	107,69	54,01	74,66	33,83	11,96
105	28,57	6,18	97,50	85,87	121,71	47,96	112,09	50,28	68,77	41,59	14,70
120	16,66	5,16	109,49	89,72	115,32	41,47	108,72	43,26	66,22	44,67	15,79

Table 4. Data of diastolic force with 10 µM Rodin A. Values of the individual muscle strips at the measure points. Specified as percentage of the BL. Calculation of the mean values, standard deviation, and standard error of the mean (SEM).

Dev. Force	131120 CH7	201120 CH7	271120 CH8	301120 CH5	111220 CH8	160221 CH6	100321 CH6	230321 CH7	Mittelwert	Stabw	SEM
Lmax (%)	100,00	100,00	100,00	100,00	100,00	100,00	100,00	100,00	100,00	0,00	0,00
15	115,91	107,60	138,91	164,73	113,61	107,53	106,36	108,13	120,35	20,88	7,38
30	146,01	122,21	148,21	185,47	142,70	107,65	110,89	110,84	134,25	26,66	9,42
45	160,49	125,24	149,04	205,54	135,42	107,38	114,21	103,39	137,59	33,93	12,00
60	163,57	121,36	138,72	209,48	120,34	101,74	112,26	101,19	133,58	36,90	13,04
75	158,49	115,52	124,14	201,28	104,99	98,10	110,20	93,73	125,81	36,54	12,92
90	149,50	104,14	109,03	187,42	78,88	92,72	106,56	85,52	114,22	36,50	12,90
105	139,91	88,02	90,71	161,67	73,11	85,72	105,17	80,44	103,09	31,36	11,09
120	125,81	75,50	81,00	156,00	60,69	77,20	103,69	76,13	94,50	32,01	11,32

Table 5. Data of developed force with 10 µM Rodin A. Values of the individual muscle strips at the measure points. Specified as percentage of the BL. Calculation of the mean values, standard deviation, and standard error of the mean (SEM).

Systolic Force	131120 CH7	201120 CH7	271120 CH8	301120 CH5	111220 CH8	160221 CH6	100321 CH6	230321 CH7	Mittelwert	Stabw	SEM
Lmax (%)	100,00	100,00	100,00	100,00	100,00	100,00	100,00	100,00	100,00	0,00	0,00
15	90,01	95,77	129,28	128,22	110,80	104,11	105,34	104,45	108,50	14,02	4,96
30	98,26	101,89	133,64	137,44	134,72	102,94	109,08	102,69	115,08	17,01	6,01
45	108,08	103,93	131,31	161,81	130,44	101,37	112,40	94,44	117,97	22,07	7,80
60	112,51	97,89	125,39	156,13	119,11	95,95	110,64	91,54	113,64	20,82	7,36
75	106,86	89,12	117,77	147,75	107,83	93,16	109,39	86,74	107,33	19,65	6,95
90	102,26	75,83	106,80	142,16	88,03	87,79	106,69	78,84	98,55	21,32	7,54
105	91,49	57,11	92,60	126,03	84,59	80,85	106,17	74,04	89,11	20,74	7,33
120	78,34	48,94	88,84	124,84	73,59	72,59	104,40	69,15	82,59	23,34	8,25

Table 6. Data of systolic force with 10 µM Rodin A. Values of the individual muscle strips at the measure points. Specified as percentage of the BL. Calculation of the mean values, standard deviation, and standard error of the mean (SEM).

dP/dtmax	131120 CH7	201120 CH7	271120 CH8	301120 CH5	111220 CH8	160221 CH6	100321 CH6	230321 CH7	Mittelwert	Stabw	SEM
Lmax (%)	100,00	100,00	100,00	100,00	100,00	100,00	100,00	100,00	100,00	0,00	0,00
15	133,59	106,40	143,73	137,38	126,99	109,29	111,40	112,40	122,65	14,51	5,13
30	156,45	117,24	158,35	147,17	168,88	109,45	118,26	116,51	136,54	23,52	8,32
45	163,10	119,20	160,38	158,96	161,21	109,23	122,12	110,31	138,06	24,81	8,77
60	162,99	117,49	152,84	161,69	143,93	103,06	119,31	108,87	133,77	24,31	8,60
75	158,26	114,33	139,68	158,81	126,61	99,45	116,20	101,66	126,87	23,38	8,27
90	150,93	106,06	121,48	150,63	97,24	93,77	111,96	94,38	115,81	23,54	8,32
105	144,74	92,24	106,69	136,40	90,56	87,05	110,34	89,76	107,22	22,31	7,89
120	134,83	80,60	97,72	129,46	79,90	78,36	109,03	85,65	99,44	22,74	8,04

Table 7. Data of dP/dt_{max} with 10 µM Rodin A. Values of the individual muscle strips at the measure points. Specified as percentage of the BL. Calculation of the mean values, standard deviation, and standard error of the mean (SEM).

dP/dtmin	131120 CH7	201120 CH7	271120 CH8	301120 CH5	111220 CH8	160221 CH6	100321 CH6	230321 CH7	Mittelwert	Stabw	SEM
Lmax (%)	100,00	100,00	100,00	100,00	100,00	100,00	100,00	100,00	100,00	0,00	0,00
15	162,53	106,80	153,06	165,81	168,28	103,13	93,06	109,25	132,74	32,37	11,44
30	210,55	117,32	166,63	178,12	207,08	104,80	96,00	111,59	149,01	47,04	16,63
45	229,87	117,67	152,70	192,77	201,77	105,31	99,23	104,09	150,43	51,58	18,24
60	232,75	111,76	135,10	198,40	186,01	102,46	97,11	101,12	145,59	52,73	18,64
75	224,96	105,92	125,49	192,30	167,34	100,68	94,93	92,63	138,03	50,52	17,86
90	211,95	95,55	112,89	184,08	127,98	98,09	91,84	84,11	125,81	47,15	16,67
105	198,13	83,29	105,72	167,59	125,29	93,51	90,44	78,41	117,80	43,45	15,36
120	179,23	71,12	96,98	163,97	109,08	87,09	89,17	73,80	108,80	40,79	14,42

Table 8. Data of dP/dt_{min} with 10 µM Rodin A. Values of the individual muscle strips at the measure points. Specified as percentage of the BL. Calculation of the mean values, standard deviation, and standard error of the mean (SEM).

RT 50%											
TFall (ms)	131120 CH7	201120 CH7	271120 CH8	301120 CH5	111220 CH8	160221 CH6	100321 CH6	230321 CH7	Mittelwert	Stabw	SEM
Lmax (%)	100,00	100,00	100,00	100,00	100,00	100,00	100,00	100,00	100,00	0,00	0,00
15	69,39	100,41	93,81	94,05	70,61	103,62	108,57	98,45	92,36	14,62	5,17
30	69,02	104,56	90,78	96,26	69,97	103,23	112,45	99,35	93,20	15,94	5,63
45	69,76	107,28	93,89	99,86	69,34	104,47	115,45	98,84	94,86	16,88	5,97
60	70,61	107,50	100,00	99,14	67,68	100,48	114,91	97,68	94,75	16,79	5,94
75	70,13	105,59	103,20	99,53	65,92	97,63	114,69	98,45	94,39	17,19	6,08
90	70,61	111,80	95,44	94,83	63,15	95,24	113,76	100,39	93,15	17,91	6,33
105	70,13	108,98	81,47	90,91	61,07	91,69	113,93	100,78	89,87	18,35	6,49
120	69,04	105,59	87,68	89,66	58,99	87,21	114,09	100,18	89,06	18,26	6,46

Table 9. Data of RT50%Fall with 10 µM Rodin A. Values of the individual muscle strips at the measure points. Specified as percentage of the BL. Calculation of the mean values, standard deviation, and standard error of the mean (SEM).

Tau (ms)	131120 CH7	201120 CH7	271120 CH8	301120 CH5	111220 CH8	160221 CH6	100321 CH6	230321 CH7	Mittelwert	Stabw	SEM
Lmax (%)	100,00	100,00	100,00	100,00	100,00	100,00	100,00	100,00	100,00	0,00	0,00
15	70,59	104,13	60,14	92,98	43,34	99,84	100,07	99,89	83,87	22,83	8,07
30	67,18	111,64	52,05	96,12	41,08	99,73	100,98	99,41	83,53	26,26	9,29
45	67,12	114,47	55,56	95,87	40,64	99,79	102,16	99,43	84,38	26,35	9,32
60	68,48	110,50	57,31	94,89	40,25	99,11	104,47	100,37	84,42	25,64	9,07
75	68,82	108,98	62,63	95,74	40,29	99,13	105,78	101,74	85,39	24,96	8,83
90	69,50	106,25	72,41	93,39	40,88	98,39	106,81	101,59	86,15	23,26	8,22
105	68,17	110,45	87,51	90,91	40,46	98,02	107,57	102,36	88,18	23,47	8,30
120	71,97	110,98	97,28	90,12	42,46	96,85	108,48	103,27	90,18	22,81	8,06

Table 10. Data of Tau with 10 µM Rodin A. Values of the individual muscle strips at the measure points. Specified as percentage of the BL. Calculation of the mean values, standard deviation, and standard error of the mean (SEM).

8.2 Measured values with 250 nM IRBM-D

Diastolic Force	131120 CH6	201120 CH6	231120 CH5	251120 CH6	271120 CH7	301120 CH6	111220 CH8	150221 CH8	230321 CH6	Mittelwert	Stabw	SEM
Lmax (%)	100,00	100,00	100,00	100,00	100,00	100,00	100,00	100,00	100,00	100,00	0,00	0,00
15min	71,37	76,45	146,13	92,47	51,60	92,71	74,98	68,30	85,11	84,35	26,46	8,82
30	67,47	68,36	115,00	98,93	47,60	96,52	69,62	39,67	82,09	76,14	24,50	8,17
45	86,37	70,46	80,40	96,73	46,13	88,70	64,85	71,71	83,73	76,57	15,17	5,06
60	88,96	57,68	51,33	95,20	39,45	85,90	59,16	69,67	84,56	70,21	19,40	6,47
75	102,26	60,28	49,20	99,20	185,11	78,81	36,57	63,70	83,67	84,31	43,66	14,55
90	74,97	57,09	33,33	95,93	229,91	78,81	37,41	57,00	81,06	82,83	58,87	19,62
105	68,87	58,18	25,60	97,60		78,74	45,27	59,86	80,71	64,36	22,44	7,93
120	71,97	57,88	25,53	98,20		85,43	24,85	69,22	78,45	63,94	26,67	9,43

Table 11. Data of diastolic force with 250 nM IRBM-D. Values of the individual muscle strips at the measure points. Specified as percentage of the BL. Calculation of the mean values, standard deviation, and standard error of the mean (SEM).

Dev. Force	131120 CH6	201120 CH6	231120 CH5	251120 CH6	271120 CH7	301120 CH6	111220 CH8	150221 CH8	230321 CH6	Mittelwert	Stabw	SEM
Lmax (%)	100,00	100,00	100,00	100,00	100,00	100,00	100,00	100,00	100,00	100,00	0,00	0,00
15	210,57	99,81	104,22	97,93	126,58	119,80	168,27	110,66	102,31	126,68	38,27	12,76
30	224,94	101,72	102,42	113,94	129,15	135,08	143,59	118,20	105,49	130,50	38,37	12,79
45	239,12	100,86	99,68	127,87	113,15	138,75	169,94	122,19	116,79	136,48	44,01	14,67
60	249,31	101,72	99,20	146,55	98,91	134,13	181,21	116,24	121,64	138,77	49,28	16,43
75	243,69	96,66	98,79	167,21	83,76	121,73	155,82	120,98	120,26	134,32	49,09	16,36
90	231,89	89,25	97,35	182,18	73,22	112,05	139,97	109,12	115,15	127,80	50,11	16,70
105	218,75	78,92	93,13	152,31		100,00	124,89	105,64	108,52	122,77	44,57	15,76
120	207,95	67,77	89,82	135,68		96,62	104,71	106,02	100,54	113,64	42,51	15,03

Table 12. Data of developed force with 250 nM IRBM-D. Values of the individual muscle strips at the measure points. Specified as percentage of the BL. Calculation of the mean values, standard deviation, and standard error of the mean (SEM).

Systolic Force	131120 CH6	201120 CH6	231120 CH5	251120 CH6	271120 CH7	301120 CH6	111220 CH8	150221 CH8	230321 CH6	Mittelwert	Stabw	SEM
Lmax (%)	100,00	100,00	100,00	100,00	100,00	100,00	100,00	100,00	100,00	100,00	0,00	0,00
15	165,72	97,82	117,12	96,49	112,38	110,45	143,07	86,09	98,85	114,22	25,30	8,43
30	174,17	98,87	106,30	110,24	113,72	121,78	140,56	72,64	100,79	115,45	28,63	9,54
45	189,87	98,17	93,78	120,35	100,46	121,48	141,56	92,91	110,14	118,75	31,05	10,35
60	197,61	97,82	84,56	134,23	87,65	117,49	148,23	89,21	114,19	119,00	36,74	12,25
75	198,07	93,46	83,60	150,98	102,96	106,92	123,64	87,75	112,90	117,81	36,41	12,14
90	181,30	86,45	77,09	161,64	102,90	100,58	112,27	78,90	108,29	112,16	36,16	12,05
105	170,43	77,12	71,69	139,24		92,66	103,37	79,08	102,93	104,56	34,16	12,08
120	164,11	66,92	70,12	126,66		92,96	83,12	84,67	96,09	98,08	32,43	11,47

Table 13. Data of systolic force with 250 nM IRBM-D. Values of the individual muscle strips at the measure points. Specified as percentage of the BL. Calculation of the mean values, standard deviation, and standard error of the mean (SEM).

dP/dtmax	131120 CH6	201120 CH6	231120 CH5	251120 CH6	271120 CH7	301120 CH6	111220 CH8	150221 CH8	230321 CH6	Mittelwert	Stabw	SEM
Lmax (%)	100,00	100,00	100,00	100,00	100,00	100,00	100,00	100,00	100,00	100,00	0,00	0,00
15	211,96	105,13	97,41	98,64	130,88	106,88	183,55	111,80	105,52	127,98	41,35	13,78
30	226,01	108,32	93,32	108,43	131,71	113,18	170,53	116,54	110,22	130,92	41,82	13,94
45	234,73	108,53	91,87	123,21	116,27	113,81	206,89	111,05	122,10	136,50	49,16	16,39
60	244,52	109,42	93,76	147,87	102,48	109,97	216,10	105,33	128,36	139,76	54,20	18,07
75	238,35	104,71	95,15	174,34	84,26	100,94	183,23	105,04	128,27	134,92	52,13	17,38
90	227,71	97,28	94,76	193,56	74,46	97,72	161,48	96,08	124,31	129,71	52,68	17,56
105	214,51	87,23	91,84	162,92		91,03	144,38	87,72	118,88	124,81	46,19	16,33
120	204,89	76,45	87,30	146,06		92,33	122,39	83,71	111,23	115,55	42,86	15,15

Table 14. Data of dp/dt_{max} with 250 nM IRBM-D. Values of the individual muscle strips at the measure points. Specified as percentage of the BL. Calculation of the mean values, standard deviation, and standard error of the mean (SEM).

dP/dtmin	131120 CH6	201120 CH6	231120 CH5	251120 CH6	271120 CH7	301120 CH6	111220 CH8	150221 CH8	230321 CH6	Mittelwert	Stabw	SEM
Lmax (%)	100,00	100,00	100,00	100,00	100,00	100,00	100,00	100,00	100,00	100,00	0,00	0,00
15	198,14	99,91	103,81	99,70	124,89	134,28	171,30	115,87	105,53	128,16	34,77	11,59
30	220,07	99,55	106,94	114,26	122,48	151,19	214,77	124,50	109,21	140,33	46,12	15,37
45	234,15	95,63	102,04	119,56	107,52	156,88	246,73	128,50	117,51	145,39	56,79	18,93
60	236,61	94,90	98,40	118,97	92,34	154,07	250,22	124,36	119,59	143,27	59,92	19,97
75	229,23	90,08	93,98	123,03	65,74	143,19	195,02	126,10	117,44	131,54	51,80	17,27
90	218,33	83,78	91,41	132,97	64,23	134,18	170,05	116,02	112,01	124,78	46,98	15,66
105	205,20	74,26	85,05	112,05		124,37	170,09	117,91	105,78	124,34	43,46	15,36
120	194,09	64,29	81,96	99,08		119,18	153,35	119,10	97,55	116,08	41,36	14,62

Table 15. Data of dp/dt_{min} with 250 nM IRBM-D. Values of the individual muscle strips at the measure points. Specified as percentage of the BL. Calculation of the mean values, standard deviation, and standard error of the mean (SEM).

RT 50% TFall (ms)	131120 CH6	201120 CH6	231120 CH5	251120 CH6	271120 CH7	301120 CH6	111220 CH8	150221 CH8	230321 CH6	Mittelwert	Stabw	SEM
Lmax (%)	100,00	100,00	100,00	100,00	100,00	100,00	100,00	100,00	100,00	100,00	0,00	0,00
15	102,50	98,04	101,09	107,64	99,55	80,60	92,91	115,12	96,34	99,31	9,58	3,19
30	104,88	100,49	98,51	105,88	103,49	81,95	58,24	116,67	94,99	96,12	16,99	5,66
45	105,69	102,94	99,04	116,46	103,22	80,09	61,02	118,91	96,96	98,26	17,95	5,98
60	105,40	103,76	100,00	121,12	103,49	79,38	63,99	125,00	99,27	100,16	18,87	6,29
75	105,69	101,72	106,13	116,73	116,30	78,68	68,22	121,21	100,78	101,72	17,70	5,90
90	109,37	101,10	106,72	119,52	112,75	78,08	71,70	118,42	99,64	101,92	16,83	5,61
105	109,10	100,94	109,22	117,42		74,49	66,56	112,28	100,49	98,81	18,44	6,52
120	111,04	101,10	106,34	121,49		74,40	64,25	101,96	99,54	97,52	18,95	6,70

Table 16. Data of RT50%TFall with 250 nM IRBM-D. Values of the individual muscle strips at the measure points. Specified as percentage of the BL. Calculation of the mean values, standard deviation, and standard error of the mean (SEM).

Tau (ms)	131120 CH6	201120 CH6	231120 CH5	251120 CH6	271120 CH7	301120 CH6	111220 CH8	150221 CH8	230321 CH6	Mittelwert	Stabw	SEM
Lmax (%)	100,00	100,00	100,00	100,00	100,00	100,00	100,00	100,00	100,00	100,00	0,00	0,00
15	91,56	103,22	102,26	89,86	98,48	94,34	106,57	86,46	102,12	97,21	6,93	2,31
30	88,02	107,32	95,57	91,47	99,40	95,54	75,20	94,55	103,09	94,46	9,27	3,09
45	88,75	111,94	99,02	96,86	102,24	96,59	66,10	99,96	103,72	96,13	12,87	4,29
60	92,48	112,91	101,74	109,88	103,11	97,93	67,69	99,82	104,74	98,92	13,20	4,40
75	93,25	113,44	113,30	121,58	113,04	97,57	72,97	96,16	103,59	102,77	14,72	4,91
90	92,80	112,50	115,66	126,65	136,88	99,16	86,31	106,23	105,14	109,04	15,98	5,33
105	93,01	113,00	120,42	123,84		98,17	104,70	104,54	106,63	108,04	10,53	3,72
120	97,35	112,65	121,29	124,10		105,63	122,49	92,11	111,19	110,85	11,86	4,19

Table 17. Data of Tau with 250 nM IRBM-D. Values of the individual muscle strips at the measure points. Specified as percentage of the BL. Calculation of the mean values, standard deviation, and standard error of the mean (SEM).

8.3 Measured values with 250 nM Givinostat

Diastolic Force	121120 CH8	131120 CH5	201120 CH5	231120 CH6	251120 CH5	021220 CH7	100321 CH7	Mittelwert	Stabw	SEM
Lmax (%)	100,00	100,00	100,00	100,00	100,00	100,00	100,00	100,00	0,00	0,00
15min	56,80	78,70	80,19	82,15	80,14	76,48	99,34	79,12	12,42	4,69
30	44,20	46,68	81,95	75,57	77,17	56,93	98,46	68,71	20,02	7,57
45	16,07	31,87	88,83	72,88	65,80	56,81	101,54	61,97	30,17	11,40
60	16,93	31,62	87,34	73,78	65,84	53,06	100,81	61,34	29,81	11,27
75	45,93	28,68	71,88	54,14	75,37	40,93	104,47	60,20	25,60	9,68
90		26,08	50,00	42,37	64,76	27,98	107,69	53,15	30,34	12,38
105		19,85	30,91	56,73	75,93	11,17	112,09	51,11	38,33	15,65
120		24,89	19,87	44,47	89,83	3,03	108,72	48,47	41,94	17,12

Table 18. Data of diastolic force with 250 nM Givinostat. Values of the individual muscle strips at the measure points. Specified as percentage of the BL. Calculation of the mean values, standard deviation, and standard error of the mean (SEM).

Dev. Force	121120 CH8	131120 CH5	201120 CH5	231120 CH6	251120 CH5	021220 CH7	100321 CH7	Mittelwert	Stabw	SEM
Lmax (%)	100,00	100,00	100,00	100,00	100,00	100,00	100,00	100,00	0,00	0,00
15	97,99	91,81	99,26	106,16	117,80	135,32	106,36	107,81	14,65	5,54
30	87,55	104,23	101,76	107,10	103,20	150,82	110,89	109,36	19,68	7,44
45	72,54	107,83	95,63	105,87	97,57	135,53	114,21	104,17	19,22	7,27
60	57,10	116,08	92,36	108,03	82,31	98,16	112,26	95,19	20,52	7,76
75	41,37	109,22	80,67	104,00	76,16	119,85	110,20	91,64	27,35	10,34
90		106,61	69,78	101,90	64,72	99,56	106,56	91,52	19,06	7,78
105		99,83	64,09	101,26	86,79	75,91	105,17	88,84	16,28	6,65
120		92,64	59,00	107,24	86,58	62,81	103,69	85,33	20,36	8,31

Table 19. Data of developed force with 250 nM Givinostat. Values of the individual muscle strips at the measure points. Specified as percentage of the BL. Calculation of the mean values, standard deviation, and standard error of the mean (SEM).

Systolic Force (	121120 CH8	131120 CH5	201120 CH5	231120 CH6	251120 CH5	021220 CH7	100321 CH7	Mittelwert	Stabw	SEM
Lmax (%)	100,00	100,00	100,00	100,00	100,00	100,00	100,00	100,00	0,00	0,00
15	85,58	87,98	95,47	100,72	100,30	101,02	105,34	96,63	7,34	2,78
30	74,49	87,34	97,84	99,95	78,10	96,09	109,08	91,84	12,43	4,70
45	55,52	85,53	94,29	98,37	73,11	89,64	112,40	86,98	18,35	6,94
60	44,98	96,52	94,58	100,27	74,66	71,87	110,64	84,79	22,34	8,45
75	42,75	85,56	78,93	92,70	75,81	73,84	109,39	79,86	20,41	7,72
90		82,97	65,86	88,41	64,74	57,83	106,69	77,75	18,36	7,50
105		76,35	57,51	91,15	81,73	38,17	106,17	75,18	24,26	9,90
120		72,75	51,25	93,02	88,09	27,96	104,40	72,91	28,69	11,71

Table 20. Data of systolic force with 250 nM Givinostat. Values of the individual muscle strips at the measure points. Specified as percentage of the BL. Calculation of the mean values, standard deviation, and standard error of the mean (SEM).

dP/dtmax	121120 CH8	131120 CH5	201120 CH5	231120 CH6	251120 CH5	021220 CH7	100321 CH7	Mittelwert	Stabw	SEM
Lmax (%)	100,00	100,00	100,00	100,00	100,00	100,00	100,00	100,00	0,00	0,00
15	99,24	100,74	103,49	95,52	119,20	135,33	111,40	109,28	14,01	5,30
30	90,24	109,64	107,98	96,42	104,35	148,11	118,26	110,71	18,83	7,12
45	76,29	112,23	103,49	97,53	95,82	131,45	122,12	105,56	18,30	6,92
60	63,50	120,30	101,70	100,68	77,62	96,49	119,31	97,08	20,71	7,83
75	47,73	116,59	90,22	95,94	75,43	120,43	116,20	94,65	26,46	10,00
90		116,31	80,43	92,57	63,08	100,27	111,96	94,10	20,01	8,17
105		112,88	76,48	92,95	94,69	79,25	110,34	94,43	15,16	6,19
120		108,53	72,69	90,50	93,39	67,36	109,03	90,25	17,49	7,14

Table 21. Data of dp/dt_{max} with 250 nM Givinostat. Values of the individual muscle strips at the measure points. Specified as percentage of the BL. Calculation of the mean values, standard deviation, and standard error of the mean (SEM).

dP/dtmin	121120 CH8	131120 CH5	201120 CH5	231120 CH6	251120 CH5	021220 CH7	100321 CH7	Mittelwert	Stabw	SEM
Lmax (%)	100,00	100,00	100,00	100,00	100,00	100,00	100,00	100,00	0,00	0,00
15	89,95	100,48	97,45	106,92	113,53	131,37	93,06	104,68	14,24	5,38
30	78,17	118,61	104,38	109,78	101,40	142,86	96,00	107,31	20,07	7,59
45	61,24	120,14	95,91	109,53	100,00	121,11	99,23	101,02	20,23	7,64
60	53,81	125,69	92,86	111,59	86,71	86,61	97,11	93,48	22,53	8,52
75	43,17	117,76	79,81	108,19	71,39	113,13	94,93	89,77	26,78	10,12
90		112,08	68,35	107,41	59,35	91,94	91,84	88,50	20,94	8,55
105		103,91	62,32	106,51	68,60	68,78	90,44	83,43	19,40	7,92
120		95,63	57,88	110,56	67,35	55,44	89,17	79,34	22,41	9,15

Table 22. Data of dp/dt_{min} with 250 nM Givinostat. Values of the individual muscle strips at the measure points. Specified as percentage of the BL. Calculation of the mean values, standard deviation, and standard error of the mean (SEM).

RT 50% TFall (ms)	121120 CH8	131120 CH5	201120 CH5	231120 CH6	251120 CH5	021220 CH7	100321 CH7	Mittelwert	Stabw	SEM
Lmax (%)	100,00	100,00	100,00	100,00	100,00	100,00	100,00	100,00	0,00	0,00
15	106,62	60,73	102,13	95,54	105,19	102,86	108,57	97,38	16,69	6,31
30	112,97	61,47	99,19	94,83	128,38	107,74	112,45	102,43	21,05	7,96
45	116,18	62,91	97,07	93,10	114,96	112,43	115,45	101,73	19,54	7,38
60	111,76	62,46	98,50	94,27	95,04	114,46	114,91	98,77	18,39	6,95
75	91,50	66,23	99,64	92,36	172,73	106,64	114,69	106,25	33,03	12,49
90		68,83	98,71	90,33	183,80	108,39	113,76	110,64	39,17	15,99
105		71,80	98,97	91,13	140,50	110,75	113,93	104,51	23,25	9,49
120		74,90	97,00	90,90	130,58	114,26	114,09	103,62	19,90	8,12

Table 23. Data of RT50%TFall with 250 nM Givinostat. Values of the individual muscle strips at the measure points. Specified as percentage of the BL. Calculation of the mean values, standard deviation, and standard error of the mean (SEM).

Tau (ms)	121120 CH8	131120 CH5	201120 CH5	231120 CH6	251120 CH5	021220 CH7	100321 CH7	Mittelwert	Stabw	SEM
Lmax (%)	100,00	100,00	100,00	100,00	100,00	100,00	100,00	100,00	0,00	0,00
15	99,77	95,28	96,30	98,27	90,12	102,03	100,07	97,41	3,95	1,49
30	102,07	95,09	88,55	95,48	94,83	111,48	100,98	98,35	7,31	2,76
45	116,87	101,49	90,36	95,64	92,15	118,92	102,16	102,51	11,39	4,31
60	137,98	104,53	91,37	97,05	95,27	134,09	104,47	109,25	18,94	7,16
75		110,60	95,29	98,23	103,58	114,28	105,78	104,63	7,20	2,94
90		115,28	100,29	101,20	105,50	118,13	106,81	107,87	7,33	2,99
105		119,53	103,58	101,55	105,12	124,67	107,57	110,34	9,46	3,86
120		123,22	105,23	106,23	105,31	135,57	108,48	114,00	12,60	5,14

Table 24. Data of Tau with 250 nM Givinostat. Values of the individual muscle strips at the measure points. Specified as percentage of the BL. Calculation of the mean values, standard deviation, and standard error of the mean (SEM).

8.4 Measured values with 10 µM DMSO (Control group)

Diastolic Force	121120 CH6	201120 CH8	111220 CH5	111220 CH7	150221 CH6	160221 CH5	100321 CH5	230321 CH5	Mittelwert	Stabw	SEM
Lmax (%)	100,00	100,00	100,00	100,00	100,00	100,00	100,00	100,00	100,00	0,00	0,00
15min	86,83	105,44	94,13	73,34	96,57	126,46	84,12	143,54	101,30	23,28	8,23
30	74,76	86,04	91,30	60,88	88,80	176,60	64,04	153,29	99,46	42,36	14,98
45	77,16	100,56	93,86	39,60	59,89	246,54	65,00	160,53	105,39	67,56	23,88
60	73,29	78,24	86,58	36,99	73,14	239,49	77,51	89,60	94,36	60,80	21,50
75	76,29	36,12	91,44	24,70	72,80	223,01	76,79	63,31	83,06	60,76	21,48
90	81,16	27,52	64,67	17,86	100,69	189,89	67,84	64,79	76,80	52,99	18,73
105		28,56	73,36	18,75	69,03	130,05	75,47	54,13	64,19	36,53	13,81
120		24,00	71,14	7,24	56,46	161,17	77,03	53,88	64,42	49,40	18,67

Table 25. Data of diastolic force with 10 µM DMSO. Values of the individual muscle strips at the measure points. Specified as percentage of the BL. Calculation of the mean values, standard deviation, and standard error of the mean (SEM).

Dev. Force	121120 CH6	201120 CH8	111220 CH5	111220 CH7	150221 CH6	160221 CH5	100321 CH5	230321 CH5	Mittelwert	Stabw	SEM
Lmax (%)	100,00	100,00	100,00	100,00	100,00	100,00	100,00	100,00	100,00	0,00	0,00
15	103,50	106,55	101,58	114,15	98,00	113,04	94,77	110,58	105,27	7,06	2,50
30	81,25	114,18	93,32	112,64	104,08	139,67	94,90	111,68	106,47	17,63	6,23
45	68,75	121,83	82,78	111,39	105,02	147,63	90,22	103,94	103,95	24,38	8,62
60	56,36	106,17	74,70	99,50	102,94	141,51	84,78	91,48	94,68	25,05	8,86
75	44,07	86,68	67,28	77,72	96,65	128,70	81,21	84,35	83,33	24,15	8,54
90	32,18	94,15	59,74	70,90	88,81	113,49	78,39	77,69	76,92	24,24	8,57
105		93,31	54,43	44,17	81,25	97,18	76,05	75,06	74,49	19,32	7,30
120		76,91	48,29	36,01	73,61	84,18	74,87	72,52	66,63	17,51	6,62

Table 26. Data of developed force with 10 µM DMSO. Values of the individual muscle strips at the measure points. Specified as percentage of the BL. Calculation of the mean values, standard deviation, and standard error of the mean (SEM).

Systolic Force (	121120 CH6	201120 CH8	111220 CH5	111220 CH7	150221 CH6	160221 CH5	100321 CH5	230321 CH5	Mittelwert	Stabw	SEM
Lmax (%)	100,00	100,00	100,00	100,00	100,00	100,00	100,00	100,00	100,00	0,00	0,00
15	97,65	106,17	100,22	92,75	97,62	115,99	92,07	119,97	102,80	10,39	3,67
30	79,00	104,79	92,97	85,50	100,06	147,80	87,03	123,52	102,58	22,92	8,10
45	71,67	114,73	84,80	73,74	93,14	169,42	83,83	120,06	101,43	32,63	11,54
60	62,28	96,84	76,85	66,72	95,09	163,09	82,91	90,96	91,84	31,45	11,12
75	55,28	69,81	71,67	49,92	90,37	149,50	80,09	78,36	80,63	30,77	10,88
90	49,26	71,93	60,65	57,20	91,93	130,35	75,71	74,02	76,38	25,44	9,00
105		71,71	57,88	30,84	78,03	104,42	75,91	69,12	69,70	22,24	8,41
120		59,24	52,46	20,91	69,09	101,14	75,42	67,21	63,64	24,35	9,20

Table 27. Data of systolic force with 10 µM DMSO. Values of the individual muscle strips at the measure points. Specified as percentage of the BL. Calculation of the mean values, standard deviation, and standard error of the mean (SEM).

dP/dtmax	121120 CH6	201120 CH8	111220 CH5	111220 CH7	150221 CH6	160221 CH5	100321 CH5	230321 CH5	Mittelwert	Stabw	SEM
Lmax (%)	100,00	100,00	100,00	100,00	100,00	100,00	100,00	100,00	100,00	0,00	0,00
15	103,27	106,09	101,38	138,18	94,79	113,55	98,13	116,36	108,97	13,86	4,90
30	84,11	105,35	92,76	138,13	99,05	142,96	98,90	119,81	110,13	21,40	7,57
45	75,38	113,56	82,11	132,20	99,28	149,89	93,23	112,46	107,27	25,11	8,88
60	65,13	102,12	74,66	118,29	94,93	142,48	87,18	99,75	98,06	24,38	8,62
75	54,49	91,89	68,12	94,70	87,15	128,64	84,15	92,55	87,71	21,60	7,64
90	41,49	108,76	62,57	89,79	78,32	114,13	81,29	85,59	82,74	23,45	8,29
105		111,07	59,29	58,58	69,91	98,79	79,14	82,44	79,89	19,64	7,42
120		96,86	55,05	49,17	60,85	87,73	78,76	79,65	72,58	17,80	6,73

Table 28. Data of dp/dt_{max} with 10 µM DMSO. Values of the individual muscle strips at the measure points. Specified as percentage of the BL. Calculation of the mean values, standard deviation, and standard error of the mean (SEM).

dP/dtmin	121120 CH6	201120 CH8	111220 CH5	111220 CH7	150221 CH6	160221 CH5	100321 CH5	230321 CH5	Mittelwert	Stabw	SEM
Lmax (%)	100,00	100,00	100,00	100,00	100,00	100,00	100,00	100,00	100,00	0,00	0,00
15	102,32	110,90	105,29	197,32	81,13	114,60	90,55	108,54	113,83	35,51	12,55
30	74,40	120,58	96,35	204,05	77,91	137,45	86,72	107,99	113,18	42,53	15,04
45	60,22	124,50	85,63	199,73	74,37	146,16	84,02	100,93	109,44	45,77	16,18
60	46,08	107,42	75,89	175,05	71,49	141,13	80,03	90,09	98,40	41,68	14,73
75	34,27	84,67	66,89	135,12	66,02	130,07	77,22	84,06	84,79	33,52	11,85
90	27,70	82,68	57,99	118,63	58,69	117,79	74,79	78,70	77,12	30,62	10,83
105		77,95	52,78	61,33	51,43	102,54	73,14	77,13	70,90	17,77	6,72
120		58,86	48,10	47,84	48,63	89,55	71,85	74,93	62,82	16,34	6,17

Table 29. Data of dp/dt_{min} with 10 µM DMSO. Values of the individual muscle strips at the measure points. Specified as percentage of the BL. Calculation of the mean values, standard deviation, and standard error of the mean (SEM).

RT 50% TFall (ms)	121120 CH6	201120 CH8	111220 CH5	111220 CH7	150221 CH6	160221 CH5	100321 CH5	230321 CH5	Mittelwert	Stabw	SEM
Lmax (%)	100,00	100,00	100,00	100,00	100,00	100,00	100,00	100,00	100,00	0,00	0,00
15	105,76	110,16	99,42	61,45	113,00	95,43	104,37	99,18	98,60	16,11	5,70
30	127,15	98,05	97,12	58,78	125,00	94,79	105,39	100,27	100,82	21,13	7,47
45	134,51	108,09	97,89	57,99	132,72	93,24	104,83	98,38	103,46	24,12	8,53
60	147,06	110,98	99,42	59,07	136,36	92,09	103,64	98,38	105,87	27,08	9,58
75	162,22	155,17	101,71	59,65	139,16	90,09	103,36	95,72	113,39	35,41	12,52
90	133,99	141,76	104,28	61,09	141,82	88,65	103,19	93,48	108,53	28,73	10,16
105		140,28	103,24	72,06	150,90	89,91	101,20	92,49	107,15	28,30	10,70
120		146,55	101,77	76,28	154,16	90,66	101,62	91,98	109,00	29,59	11,18

Table 30. Data of RT50% TFall with 10 µM DMSO. Values of the individual muscle strips at the measure points. Specified as percentage of the BL. Calculation of the mean values, standard deviation, and standard error of the mean (SEM).

Tau (ms)	121120 CH6	201120 CH8	111220 CH5	111220 CH7	150221 CH6	160221 CH5	100321 CH5	230321 CH5	Mittelwert	Stabw	SEM
Lmax (%)	100,00	100,00	100,00	100,00	100,00	100,00	100,00	100,00	100,00	0,00	0,00
15	102,37	105,46	103,12	99,64	107,07	97,21	97,60	104,94	102,18	3,69	1,30
30	122,78	106,22	104,51	101,46	103,70	97,58	97,82	109,27	105,42	8,07	2,85
45	120,65	106,60	103,73	104,35	103,34	95,18	98,54	111,61	105,50	7,86	2,78
60	121,21	109,22	105,97	105,76	104,47	95,35	99,37	112,81	106,77	7,96	2,81
75	132,55	120,02	107,86	109,11	104,53	95,15	99,04	112,87	110,14	11,91	4,21
90		134,10	111,59	113,65	108,66	98,99	99,71	113,52	111,46	11,71	4,43
105		135,24	117,69	142,71	110,10	98,59	100,88	115,18	117,20	16,55	6,26
120		151,50	120,10	182,92	113,07	99,27	102,94	116,61	126,63	30,07	11,36

Table 31. Data of Tau with 10 µM DMSO. Values of the individual muscle strips at the measure points. Specified as percentage of the BL. Calculation of the mean values, standard deviation, and standard error of the mean (SEM).